Effects of complexation with sulfuric acid on the photodissociation of protonated Cinchona alkaloids in the gas phase

Feriel Ben Nasr, Ivan Alata, Debora Scuderi, Valéria Lepère, Valérie Brenner, Nejm-Eddine Jaïdane, Anne Zehnacker

Effects of complexation with sulfuric acid on the Photodissociation of Protonated Cinchona Alkaloids in the gas phase

Feriel Ben Nasr, [a,d] Ivan Alata, [a] Debora Scuderi,[b] Valeria Lepère, [a] Valerie Brenner,[c] Nejm-Eddine Jaïdane,[d] Anne Zehnacker [*a]

a) *Institut des Sciences Moléculaires d'Orsay (ISMO), CNRS, Univ. Paris-Sud, Université Paris-Saclay, F-91405 Orsay, France*

b) *Univ. Paris-Sud, Laboratoire de Chimie Physique, UMR8000, and CNRS, Orsay, F-91405 France*

c) *LIDYL, CEA, CNRS, F-91191 Gif-sur-Yvette, France*

d) *Laboratoire de Spectroscopie Atomique, Moléculaire et Applications (LSAMA) Université de Tunis El Manar, LSAMA, Tunis 1060, Tunisia*

*e-mail anne.zehnacker-rentien@u-psud.fr

Abstract

The role of complexation with sulfuric acid on the photodissociation of protonated cinchona alkaloids, namely cinchonidine (Cd), quinine (Qn) and quinidine (Qd), is studied by combining laser spectroscopy with quantum chemical calculations. The protonated complexes are structurally characterized in a room-temperature ion trap by means of Infra-Red Multiple Photon dissociation (IRMPD) spectroscopy in the fingerprint and the ν(XH) (X=C, N, O) stretch regions. Comparison with density functional theory calculations including dispersion (DFT-D) unambiguously shows that the complex consists of a doubly protonated cinchona alkaloid strongly bound to a bisulfate HSO_4^- anion, which bridges the two protonated sites of the cinchona alkaloid. UV excitation of the complex does not induce loss of specific photo fragments. Indeed the UV-induced fragmentation pattern is identical to that observed in collision-induced dissociation experiments. This contrasts with the photodissociation observed in the protonated monomer or dimer, for which photo-specific fragments were observed. Analysis of the nature of the first electronic transitions at the second order approximate coupled-cluster level (CC2) explains the difference in behavior of the complex relative to the monomer or dimer towards UV excitation.

Introduction

Exposure of biomolecules like proteins or DNA to UV light leads to structural damages, which in turn alter their biological functions, an exemplary case being mutagenic and carcinogenic effects caused by UV radiations on DNA.[1-3] These damages may be increased in the presence of sensitizing drugs.[4] Understanding the protection mechanisms of biomolecules against UV-induced damages has prompted numerous studies, both in the biomolecules themselves and in model systems.[5] For example, the photochemistry and photophysics of individual DNA bases have been intensively studied in solution.[6-10] The solvent, water in a biological context, plays an important role in the deactivation process, by stabilizing polar or charged species, modifying the excited-state energetics, or acting as a thermal bath. Gas-phase experiments are therefore required to get information on the molecule properties without the participation of the solvent. They have been conducted on small biomolecules such as DNA bases[11-13] and peptides and allow getting information on the photophysical processes at play in the chromophore.[8, 14-22] Many studies have been devoted to the electronic excited states of protonated biomolecules isolated in the gas phase, either under supersonic expansion conditions,[23, 24] in room-temperature ion traps,[15, 25-31] and more recently in cryogenic ion traps.[32-40] Of special interest are the aza-aromatic molecules due to their complex photophysical behavior related to several close-lying electronic transitions.[29, 30, 37, 41, 42]

We have recently studied aza-aromatic molecules, namely, cinchona alkaloids. Cinchona alkaloids, among which quinine is the most famous, originate from the bark of Cinchona trees and are widely used in chemistry or medicine.[43-48] However, photosensitizing effects have been observed in the treated patients.[49] This justifies the studies of photophysical and photochemical processes in quinine, in its free base or sulfate forms.

The cinchona alkaloids, quinine (Qn), quinidine (Qd), cinchonidine (Cd) and cinchonine (Cn) are displayed in **Figure 1.** They consist of an aliphatic bicyclic tertiary amine, the alkaloid part, which is substituted by a vinyl group at C_3 and linked to a planar aromatic quinoline ring *via* an OH-containing flexible linker C_8C_9. These natural molecules are classified into pairs, *i.e.* Qd/Qn and Cd/Cn, which only differ by the chirality of C_8 and C_9. Qd/Qn differ from Cd/Cn by the presence of a methoxy substitutent on the aromatic ring. Cinchona alkaloids contain two basic nitrogens (N_{alk} and N_{arom} in **Figure 1**). The alkaloid nitrogen N_{alk} is the most basic site and is protonated in our experimental conditions. When not specified otherwise, CdH^+ denotes cinchonidine protonated on N_{alk}. Protonation on N_{arom} will be denoted by $CdN_{arom}H^+$. Doubly protonated cinchonidine (noted CdH_2^{2+} in what follows) is formed in acidic solution (pH below <~4-5). Cinchona alkaloids possess different transitions in the near UV region. The $\pi\pi^*$ transition localized on the aromatic ring is

optically active while the nπ* transitions involving the quinoline or the alkaloid nitrogen lone pair have much weaker oscillator strength.[50, 51] Like for other aza-aromatic molecules,[30] protonation removes the nπ* excited state involving the alkaloid nitrogen lone pair from the transition manifold. This results in high fluorescence quantum yield.[52]

We have previously reported that protonated cinchona alkaloids show complex photochemical properties in the gas phase, using MS^3 experiments involving IR characterization of the UV fragments.[53-57] Based on IR spectra of the photofragments, combined with CC2 calculations, we have proposed that UV-induced C_8C_9 bond cleavage happens through conformation-dependent reactions involving coupled electron and proton transfers.[53] The mechanism is modified in the protonated dimer, for which a photo-induced proton transfer, followed by dissociation of the complex, results to a metastable molecule protonated on the aromatic nitrogen, $CdN_{arom}H^+$.[54, 57, 58]

We extend here these studies to the complexes of cinchona alkaloids with sulfuric acid. Indeed, drugs based on cinchona alkaloids are used under their sulfate form and the above-mentioned complexes are spontaneously formed in the electrospray. The complexes are studied by multistage mass spectrometry (MS^n) coupled with laser spectroscopy. We first resort to Infra-Red Multiple Photon Dissociation (IRMPD) spectroscopy, combined with quantum chemical calculations, to determine the structure of the protonated complexes of cinchona alkaloids with sulfuric acid. H_2SO_4 is a strong di-acid; in water at neutral pH, the most abundant species is SO_4^{2-} and the concentration in H_2SO_4 is negligible. In contrast, H_2SO_4 is stable in the gas phase[59, 60] while isolated HSO_4^- has never been observed. Rare gas matrices are an intermediate case in which H_2SO_4 is observed when isolated or included in a 1:1 complex with NH_3.[61] However, for more basic environments, proton transfer takes place and an ion pair containing HSO_4^- is formed.

This study first aims at defining which forms of Cd, CdH^+ or CdH_2^{2+}, and sulfuric acid, H_2SO_4, HSO_4^- or SO_4^{2-}, are contained in the protonated complex. We can exclude SO_4^{2-} because there are only two stable protonation sites in the Cd molecule. However, should we describe the complex in terms of CdH^+:H_2SO_4 or CdH_2^{2+}:HSO_4^-? Furthermore, UV irradiation only results to dissociation of the complex into protonated monomers, in contrast to protonated monomers and dimers that yield specific fragments under UV excitation. The second goal of this study is then to explain the absence of specific photofragments of the complex, in terms of structure and nature of the electronic excited states calculated at the CC2 level. The present study focuses first on Cd, and is extended to Qn and Qd, which have a methoxy substitutent on the aromatic ring. Moreover, Qn and Qd differ from each other by the chirality of C_8 and C_9, which is 8S/9R in Qn, as it is in Cd, and 8R/9S in Qd. We will assess whether the structure of the complexes or their photodissociation mechanism is affected by this change in absolute configuration.

Experimental and theoretical methods:

a) Experimental method:

The experimental set-up has been described in details elsewhere.[53] The multistage mass spectrometry (MS^n) experiments were based on a modified Paul ion trap (Bruker, Esquire 3000+).[62] Ions were generated by electrospraying a 10 μM solution of the alkaloids or their sulfate in a 50:50 water/methanol mixture, adding 2 μl of 98% formic acid to assist the protonation. The electrospray ionization (ESI) conditions were those already described for these systems.[57, 63] The alkaloids under study as well as their sulfates were obtained from Sigma-Aldrich and were used without further purification.

Collision-induced dissociation (CID) spectra were obtained in a MS^2 experiment by mass selection of the parent in a ±5 Da window. The parent was fragmented in the Paul ion trap by collision with He, applying a radiofrequency (RF) voltage of variable amplitude during 200 ms.

The IRMPD spectra were recorded resorting to a MS^2 scheme involving IR irradiation in the above-mentioned Paul ion trap, equipped with a diamond window. The spectra were recorded in the 800-1800 cm^{-1} range using the infrared free electron laser (FEL) at the "Centre Laser Infrarouge d'Orsay CLIO".[64] The spectral bandwidth was typically 1% of the central wavelength and the power of the order of 0.8W. The 2800-4000 cm^{-1} range was covered by a tabletop IR Optical Parametric Oscillator/Amplifier (OPO/OPA) (LaserVision 10 Hz repetition rate, pulses duration 4-6 ns, spectral bandwidth 3 cm^{-1}, IR power of ~ 200 mW). The IR laser was focused on the center of the trap by a parabolic Oxygen-Free High-Thermal Conductivity (OFHC) copper mirror with focal length of 350 mm. A synchronized CO_2 laser (Universal Laser system 10 W at cw operation, centered at $\lambda = 10.6$ μm) was co-focused with the FEL or OPO source to enhance the fragmentation yield.

The fourth harmonic (266 nm) of a 10 Hz Nd-YAG laser (Minilite Continuum 500 μJ/pulse, pulse duration 5 ns) was used to electronically excite the systems, hence inducing their photo-dissociation. The UV laser was slightly focused on the center of the trap by a 1000 mm focal length quartz lens. The protonated complex built from cinchonidine and sulfuric acid (m/z 324) was isolated in a 5 Da window and fragmented by irradiation at 266 nm during 1 s. The photo-fragments were isolated and characterized by IRMPD based on a MS^3 scheme reported previously.[53, 54, 58]

b) Theoretical methods:

The potential energy surface (PES) of the complexes of cinchonidine was first explored with a force field using the Maestro program, a part of the Schrödinger package.[65] Exploration with two

force fields, MMFFs and OPLS2003, generated similar structures.[66 67] These force fields were already used successfully for exploring the potential-energy surface of neutral or protonated quinine as well as its protonated dimer.[57, 68] The structures with energy below 21 kJ/mol relative to the most stable one were fully optimized within the frame of the density functional theory (DFT) including empirical dispersion (DFT-D3),[69, 70] at the B3LYP-D3/6-31++G(d,p) level[71-73] and the harmonic frequencies were calculated at the same level of theory for structures which correspond to true minima. This level is known to yield frequencies in good agreement with experimental values.[70, 72, 74, 75] The "tight" criterion and fine grid were used so that the convergence threshold was set to 6 10^{-5} and 1.5 10^{-5} au for the maximum displacements and forces, respectively. In order to take into account the anharmonicity, the harmonic frequencies were corrected by mode-dependent scaling factors. These scaling factors were determined as the average of the ratio of the experimental frequencies to the calculated values of the studied molecules as described in section c).

Basis-set superposition error (BSSE) effects on both the geometry and energetics were taken into account. The geometry optimization was performed considering the BSSE term and the energetic was calculated using the counterpoise method.[76] In what follows, the stability of the complexes is given in terms of Gibbs energy ΔG relative to the most stable structure taken as the zero of the scale. The BSSE corrections does not amount to more of 5% of the relative Gibbs energy and hardly modify the geometry. For example, the $N_{alk}H^+ \ldots O^-$ distance and $N_{alk}H^+ \ldots O^-$ angle are modified by less than 0.1 % in the most stable form of CdH_2^{2+}:HSO_4^- (*vide infra*). The difference is slightly larger for the CdH^+:$H_2SO_4^-$ complexes, 0.3% and 1% for the most stable forms. Furthermore, BSSE corrections hardly modify the calculated harmonic frequencies of the most stable form of CdH_2^{2+}:HSO_4^-. The BSSE-corrected frequencies differ only by less than 0.1% from the non-BSSE-corrected ones in the ν(XH) range, a discrepancy smaller than the experimental resolution (4 cm^{-1}). The discrepancy is slightly larger in the fingerprint region, but remains smaller than 0.3%, except for the $\beta(N_{alk}H^+)$ mode (0.6%). The intermolecular modes are more affected (1 to 3%). The most modified mode is the hindered rotation of HSO_4^- (cogwheel motion) for which the discrepancy between the two calculated frequencies is 5%.

Quinine and quinidine differ from cinchonidine by the presence of a methoxy OCH_3 substituent in the aromatic ring. This leads to additional conformational flexibility, with two classes of conformers corresponding to the OCH_3 in cis or trans position, as observed in 2-methoxynaphthalene.[77] The complexes containing quinine and quinidine were then calculated using those containing cinchonidine as starting points. The chirality of the chiral centers was modified when necessary and the methoxy group was added, in the two possible positions.

The calculations were done using the Gaussian 09 package.[78] Obtained conformers structures were drawn with the Gabedit software.[79] Assignment was based on spectroscopic criteria (good match between calculated and experimental frequencies) and thermodynamics, favoring the most stable structures.

The electronic excited states of the protonated monomers and complexes were calculated at the CC2 level of theory.[80] The calculations were performed using the resolution-of-the-identity (RI) approximation[81] and the correlation-consistent polarized valence double-ζ (cc-pVDZ) basis set.[82] The ground state of the most stable structure assigned to the experiment was calculated at the RI-CC2 level, keeping the DFT-D geometry. Vertical excitation energies were then calculated at the RI-CC2 level considering six excited states. 22 core orbitals were frozen for the protonated cinchonidine monomers and 31 for the complex. The CC2 convergence was set at 10^{-7}. This method has been used on numerous protonated organic molecules and satisfactorily reproduces the $S_{1\leftarrow 0}$ transition energy.[83] All the calculations were done using the Turbomole V6.6 program package.[84] The difference in density between the ground state and the electronic excited states were calculated using the density analysis of Turbomole and plotted using the VMD software.[85]

c) Isolated systems

The vibrational spectroscopy of the molecular sub-units is summarized here. Comparison between the experimental vibrational frequencies determined previously or in this work and those calculated here are used for determining the scaling factors used.

H_2SO_4 and HSO_4^-: The vibrational spectroscopy of H_2SO_4 is well known in the gas phase[59, 60] and in low-temperature matrices.[86] In the 3 μm region, the infra-red spectrum of H_2SO_4 vapours shows an intense band at 3609.2 cm^{-1} assigned to the ν(OH) stretch.[59] The scaling factor in this range is determined as the ratio between experimental and calculated (3755 cm^{-1}) frequencies of the H_2SO_4 ν(OH) stretch, it amounts to 0,961. This scaling factor is of the same order as those defined for the B3LYP functional associated with other Pople basis sets.[87]

The experimental spectrum of H_2SO_4 in the fingerprint region (800-1800 cm^{-1}) is dominated by two intense features at 1220.1 and 1464.7 cm^{-1} assigned to the $\nu(SO_2)$ symmetric and antisymmetric stretches, respectively. The band located at 1157.1 cm^{-1} is assigned to the β(SOH) asymmetric bend while that at 834.1 and 891.4 cm^{-1} are attributed to the $S(OH)_2$ symmetric and asymmetric stretches. As we shall see later, the vibrational modes of the complexes involve stretching and bending motions extensively delocalized on the OH and CO groups. For this reasons, we have treated the stretching and bending modes on the same footing. The scaling factor in the

fingerprint region is determined as the average ratio between experimental and calculated frequencies of the $\beta(SO_2)$ and $\beta(OH)$ bends, and $\nu_S(OH)_2$ and $\nu(SO_2)$ stretches. The obtained scaling factor is 1,060. This value reproduces well the experimental IR spectra of H_2SO_4 in the low frequencies region and scaling factors >1 are generally used for SO containing species.[88-90]

Less is known on the infrared spectroscopy of the bisulfate anion HSO_4^-, which has been studied mostly in the condensed phase, for example in sulfuric acid solutions[91, 92] or thin films,[93] or in strongly bound complexes under cryogenic matrix[61] or gas-phase conditions.[90] Due to the absence of experimental data in isolated conditions, we will use the same scaling factors as for H_2SO_4.

CdH^+, QnH^+ and QdH^+: The conformational landscape of neutral cinchona alkaloids has been extensively studied by Bürgi *et al.* and Caner *et al.*[94-96] The same nomenclature as for the neutral systems is used for all protonated states,[97] as described previously.[53] The details of the nomenclature are given in the electronic supplementary information (ESI†). Briefly, the structures can be separated in two classes: in the "Closed" structures, the alkaloid is folded over the aromatic ring while in the "Open" structures, it is extended outwards.

The vibrational spectroscopy of gas-phase Cd is not known. However, Qn and Qd have been studied previously under jet-cooled conditions by IR-UV double resonance spectroscopy.[68] The experimental frequency of 3650 cm^{-1} observed in both molecules, a typical free ν(OH) stretch value, has been assigned to the ν(OH) stretch of the most stable γ-open conformer for which the calculated value is 3821 cm^{-1}, which leads to a scaling factor of 0.955. The experimental ν(OH) frequency does not change much upon protonation on the alkaloid nitrogen; it is measured at ~3650 cm^{-1} in CdH^+, QnH^+, or QdH^+ by IRMPD spectroscopy.[56] It does not change substantially with the protonation on the aromatic nitrogen and appears at the same value in $CdN_{arom}H^+$. The average scaling factor of the ν(OH) stretch of the protonated species is then taken equal to 0.955, the same value as determined for neutral Qn under supersonic-jet conditions.

The $\nu(N_{alk}H^+)$ stretch frequency is sensitive to conformation and hydrogen bond formation.[56] The cinchonidine protonated monomers and dimers ($\nu(N_{alk}H^+)$ stretch frequency ranging from 3209 to 3300 cm^{-1}) were used to determine the average scaling factor, which amounts to 0.970.[54]

The $\nu(N_{arom}H^+)$ stretch is experimentally observed at 3470 cm^{-1}, in the monomer and the dimer. The calculated value does not depend on the conformer and yields a scaling factor of 0.971.

We can anticipate from what is known on the isolated systems that free ν(OH) stretches should appear around 3650 cm^{-1} whatever the protonation state of the molecule. For protonation on N_{alk}, $\nu(N_{alk}H^+)$ is expected at 3280 cm^{-1} for a free $N_{alk}H^+$ and strongly shifted down in energy when it is involved in an intermolecular hydrogen bond.[56] Finally, for protonation on N_{arom}, $\nu(N_{arom}H^+)$ is expected around 3470 cm^{-1} range and is not sensitive to the environment.[58] The standard deviation

between calculated and experimental frequencies of the reference structures allow us to assume an error of ~20 cm^{-1} on the calculated frequencies.

Results:

1. Structural studies

1.1. Experimental IRMPD spectra

The IRMPD spectra obtained by electro-spraying a solution of cinchonidine sulfate are shown in **Figure 3 and Figure 5**. The 3 μm region shows two narrow bands in the region of the free ν(OH). The presence of two bands in this region allows ruling out the presence of SO_4^{2-}; one of these bands belongs to CdH^+ and the other one to H_2SO_4 or HSO_4^-. The band at 3652 cm^{-1} is typical of the free ν(OH) of Cd but is not informative about the protonation site of Cd. The intense band at 3621 cm^{-1} appears in the range of the free ν(OH) of H_2SO_4 or HSO_4^-, but does not allow deducing whether the system contains H_2SO_4 or HSO_4^-. Finally, a broad band appears at 3396 cm^{-1}. This range corresponds either to $\nu(N_{arom}\ H^+)$ or to intermolecular hydrogen-bonded ν(OH). We will therefore consider the two species H_2SO_4 and HSO_4^- and calculate both CdH^+:H_2SO_4 and CdH_2^{2+}:HSO_4^- complexes. The fingerprint region is dominated by an intense band centered at 1040 cm^{-1} followed by congested features spreading up to 1400 cm^{-1}.

1.2. Calculated structure of the CdH^+:H_2SO_4 complex

The most stable structures of the complexes are presented in **Figure 2**. The most important structural parameters are listed in **Table 1** and the relative energies in **Table 3**.

All the calculated conformations are strongly bound by an intermolecular $NH^{+\delta q}\ldots{}^{-\delta q'}O$ interaction that links $N_{alk}H^+$ and the SO group of sulfuric acid (d=1.84 to 1.88 Å). NBO analysis of the electron density and orbital populations is reported in the ESI† and shows that this interaction is mostly electrostatic in nature. It manifests itself by a substantial red shift of the $\nu(N_{alk}H^+)$ stretch frequency at 3291 cm^{-1}, while the ν(OH) frequencies remain unchanged relative to the bare molecules, reflecting the free nature of the H_2SO_4 hydroxyls.

In Anti-γ-open', one of the OH groups of H_2SO_4 interacts with the aromatic ring, more precisely the C_6 ring without nitrogen, denoted as $arom_C$ in what follows ($OH\ldots\pi_{aromC}$ interaction). The OH…X distance, where X is the center of the $arom_C$ ring, is 3.30 Å. Due to this interaction, the ν(OH) frequency of the interacting OH group of H_2SO_4 is shifted down in energy to 3429 cm^{-1}.

The complexes with the Closed conformers are more compact, with shorter distances between H_2SO_4 and the aromatic ring. Anti-γ-closed and Anti-γ-closed' exhibit an OH…π_{aromC} interaction, with a OH…X distance of 2.58 Å, much shorter than in Anti-γ-open'. In Anti-γ-closed', a strong OH…N_{arom} hydrogen bond bridges H_2SO_4 and the aromatic nitrogen (d=1.58 Å). This interaction results to a strong down shift of the H_2SO_4 ν(OH) frequency, down to 2343 cm^{-1}.

The calculated spectra of the CdH^+:H_2SO_4 structures are shown in **Figure 3**. The free ν(OH) stretches localized on CdH^+ and H_2SO_4 are calculated in the 3550-3650 cm^{-1} range for all the structures. When one hydroxyl group of H_2SO_4 interacts with the aromatic π electrons, like in Anti-γ-open', its ν(OH) frequency is shifted down to the 3400-3450 cm^{-1} range. When one hydroxyl group of H_2SO_4 interacts with N_{arom}, its ν(OH) frequency is shifted further down to ~ 3300 cm^{-1} in Anti-γ-closed' and 2343 cm^{-1} in Anti-γ-closed, which is out of our experimental range and is not presented in **Figure 3**. The ν($N_{alk}H^+$) stretch is calculated in the 3170-3270 cm^{-1} range in all the CdH^+:H_2SO_4 complexes indicating that it is involved in a strong interaction.

In the fingerprint region, the two β(OH) bending modes of H_2SO_4 are calculated in the 1150-1200 and 1250-1300 cm^{-1} range. They are the most intense calculated transitions, together with the ν(S-OH) stretch at ~900 cm^{-1} and the two ν(SO) stretches in the 1300- 1450 cm^{-1} region.

1.3. Calculated structure of the CdH_2^{2+}:HSO_4^- complex

The most stable structures of the CdH_2^{2+}:HSO_4^- complex are presented in **Figure 4.** The structural parameters are listed in **Table 2** and the energies in **Table 3**. Two of these complexes contain the Open form of CdH_2^{2+} and three the Closed form. They all involve strong electrostatic interactions between the bisulfate anion and the protonated nitrogen atoms. These interactions are mostly electrostatic, like that described above. The electrostatic interactions between two charged species being stronger than that between a charged species and a neutral entity. All the CdH_2^{2+}:HSO_4^- complexes are then much more stable than the corresponding CdH^+:H_2SO_4 structures, the energy difference between them being 7 kcal/mol or more.

The structures containing Open and Closed conformations of CdH_2^{2+} strongly differ from each other. When CdH_2^{2+} is Open, stabilization mostly arises from the $N_{alk}H^{+\delta q}$…$^{-\delta q'}$O interaction. This ionic interaction is strong, as it can be assessed from the short (1.58 Å) distance between $N_{alk}H^{+\delta q}$ and $O^{-\delta q'}$, and purely electrostatic. The quinoline ring and HSO_4^- are distant by more than 6.0 Å. The Anti-β-open structure involves an additional OH…$O^{-\delta q'}$ hydrogen bond relative to Syn-γ-open, from the OH of CdH_2^{2+} to one oxygen atom of HSO_4^-. The corresponding OH…$O^{-\delta q'}$ distances are 1.87 and 4.11 Å in Anti-β-open and Syn-γ-open, respectively. This hydrogen bond

contributes to the stabilization of Anti-β-open, which is more stable than the Syn-γ-open by ~ 2 kcal/mol.

The complexes with the Closed conformers involve an additional interaction between $O^{-\delta q'}$ of HSO_4^- and the $N_{arom}H^+$ group of CdH_2^{2+}, which allows HSO_4^- to bridge the two protonated nitrogen atoms. This interaction is not as strong as $N_{alk}H^{+\delta q}\ldots O^{-\delta q'}$, because of the larger (> 2.3 Å) distance between the two sites. Again, it is purely electrostatic. The geometry of the complex results from a compromise between these two interactions, but that involving the $N_{alk}H^+$ group is dominant and dictates the $N_{alk}H^{+\delta q}\ldots O^{-\delta q'}$ distance, quasi identical (1.64 to 1.60 Å) to that calculated for the Open complexes (1.58 to 1.57 Å). The $N_{arom}H^{+\delta q}\ldots O^{-\delta q'}$ interaction stabilizes the complexes containing Closed forms by more than 2 kcal/mol relative to those with Open forms.

The spectra calculated for the Cd_2H^{2+}: HSO_4^- structures are shown in **Figure 5**. The ν(OH) stretches localized on Cd_2H^{2+} and HSO_4^- are calculated in the 3580-3680 cm^{-1} range, as expected for free OH, for all the structures, except Anti-β-open in which the Cd_2H^{2+} ν(OH) is shifted down to 3380 cm^{-1} because the OH group acts as an hydrogen bond donor to an oxygen of HSO_4^-. The spectrum of Syn-γ-open stands out by the presence of an intense transition at 3106 cm^{-1} due to the aromatic $\nu(C_3,H)$ stretching mode gaining intensity through the interaction with the HSO_4^- ion. The calculated spectrum of all the complexes shows an intense $\nu(N_{alk}H^+)$ stretch in the 2570 - 2700 cm^{-1} region, which is out of our experimental range and not shown in Figure 5. [56]

The calculated $\nu(N_{arom}H^+)$ does not vary much with the structure and is calculated at ~ 3465-3470 cm^{-1} for the complexes with both Open and Closed structures. It is only shifted down by a few wavenumbers (<5 cm^{-1}) in the bridged complexes with the Closed forms, with a slightly lower value in Syn-γ-closed' than Anti-γ-closed, in line with the more compact structure of the former.

Most of the peaks calculated in the fingerprint region correspond to vibrations localized on HSO_4^-. Syn-γ-closed', Anti-γ-closed and Anti-β-open have vibrations at 1162, 1246 and 1295 cm^{-1} that are described in terms of the β(OH) bending motion of HSO_4^- coupled with ν(SO) stretches. Syn-γ-open and Syn-γ-closed have several vibrations between 1170 and 1210 cm^{-1} that correspond to the β(OH) bending motion of HSO_4^- coupled with $\beta(C_{aliphatic}H)$ and $\beta(C_{aromatic}H)$ bending motions.

1.4. Assignment of the observed complex

Figure 3 compares the experiment to the spectra simulated for CdH^+:H_2SO_4. The calculated spectrum of CdH^+:H_2SO_4 poorly reproduces the experimental data in the high frequencies range as well as in the fingerprint region. In particular, no band is observed in the range of the calculated bonded $\nu(N_{alk}H^+)$ (3170-3300 cm^{-1} range). In the fingerprint region, no strong band is observed

above 1350 cm^{-1} where the two ν(SO) stretches are expected. This result allows ruling out that the observed complex is CdH^+:H_2SO_4.

Figures 5 compares the experiment to the spectra simulated for CdH_2^{2+}:HSO_4^-. In the high frequency region, the band around 3650 cm^{-1} is assigned to a free ν(OH) stretch of CdH_2^{2+}. This allows ruling Anti-β-open for the attribution. The strong feature at 3621 cm^{-1} is attributed to ν(OH) of HSO_4^- and is only slightly lower in frequency than the free ν(OH), estimated at 3650 cm^{-1} in HSO_4^-. The broader feature around 3400 cm^{-1} is attributed to the ν($N_{arom}H^+$) stretch. Finally, no intense band is experimentally observed in the 3000-3200 cm^{-1} region corresponding to the ν(CH) stretching modes. Thus, the observed complex cannot be Syn-γ-open. Based on the 3μm region, we can safely assign the observed complex to one of the calculated structures containing a Closed conformer, which all reproduce reasonably well the experimental spectrum. The experimental spectrum obtained in the fingerprint region is also satisfactorily reproduced by those calculated for the Closed structures and most of the observed peaks are assigned to transitions localized on HSO_4^-. Moreover, the energetic values listed in **Table 3** indicate that the Closed structures are by far more stable than the complexes involving neutral H_2SO_4, and more stable by several kcal/mol than the Open conformers. Anti-γ-closed, Syn-γ-closed' and Syn-γ-closed are almost iso-energetic within the error. Among them, Syn-γ-closed' displays the best match with the experimental spectrum both in the 3 μm and in the fingerprint region. We therefore assume that the observed spectrum is mainly due to Syn-γ-closed', without excluding a contribution of the two other forms.

1.5. Extension to quinine and quinindine

The geometries obtained for QnH_2^{2+}:HSO_4^- are shown in **Figure 6** and **Figure 7**. The dihedral angles of the calculated complexes are listed in **Table 4** and **Table 5** and their energetics in **Table 6**. The structures obtained for QdH_2^{2+}:HSO_4^- are very similar and are shown in **Figure S1**. The energetics and the structural parameters are listed in **Tables S1** and **Table S2** of the ESI†.

The calculated complexes are similar for the cis and trans structures and resemble those obtained for CdH_2^{2+}:HSO_4^-. The presence of the OCH_3 substituent slightly modifies the energetic order between the different geometries and complexes with Open forms become energetically competitive with the complexes with Closed forms. The complexes built from the Closed cis conformers resemble those obtained for CdH_2^{2+}:HSO_4^-, with HSO_4^- bridging the two protonated sites of the molecule and showing no interaction with the OH or the OCH_3 groups of Qn. Cis and Trans syn-γ-Open show no difference relative to the CdH_2^{2+}:HSO_4^- system. In contrast, the Cis-anti-β-Open structure slightly differs from its counterpart in CdH_2^{2+}:HSO_4^- because HSO_4^- interacts not

only with the $N_{alk}H^+$ group but also with the OCH_3 group (distance of 2 Å) and the OH group of QnH_2^{2+}. These additional hydrogen bonds contribute to the stability to the complex. In Trans-syn-β-open, only the additional interaction between HSO_4^- and OH is observed.

The IR spectra of all these complexes, the 3μ region and the fingerprint region, are presented in **Figures 8** and **9**. In the 3 μm region, the spectra of the cis/trans QnH_2^{2+}:HSO_4^- complexes parallel those of the CdH_2^{2+}:HSO_4^- complex. In the fingerprint region, the calculated spectra of cis/trans QnH_2^{2+}:HSO_4^- have some transitions in common with CdH_2^{2+}:HSO_4^-. Most of the differences between QnH_2^{2+}:HSO_4^- and CdH_2^{2+}:HSO_4^- are due to modes localized on the methoxy substituent. The ν(CO) stretch of the OCH_3 is calculated between ~ 1110 cm^{-1} and ~ 1220 cm^{-1}, with a weak intensity. It is higher in energy and has larger intensity in the trans forms. No particularly intense band stands out in the cis conformers. A very intense β($C_{arom}H$) bend is calculated at ~ 1300 cm^{-1} - 1330 cm^{-1} for all the trans conformers of QnH_2^{2+}, becoming the most intense in the fingerprint region. The absence of intense transition in the ~ 1400 cm^{-1} region of the experimental spectrum and the presence of bands above 1650 cm^{-1} allows discarding the trans conformers.

The results obtained in the high-frequency region parallel those obtained for cinchonidine. The spectrum of the Closed cis geometries shows better correspondence with the experimental data than those of the Open cis geometries. Moreover, the cis conformers are more stable than the trans. Cis-Syn-γ-closed, Cis-Syn-γ-closed' and Cis-Anti-γ-closed show good correspondence with the experiment. It is therefore likely that the observed spectrum contains contributions of these three cis Closed forms, whose relative Gibbs energy (1.0-1.5 kcal/mol) is of the order of the expected calculation error. The preference for cis forms results parallel those observed for similar systems like neutral 2-methoxynaphthalene [77], Naproxene, [98, 99] or neutral quinine and hydroquinine. [68, 97]

No difference is experimentally observed between the complexes Qn and Qd, as it was already the case for the protonated monomers.[56] Qn and Qd therefore behave like true enantiomers in this context.

2. Photodissociation

2.1. Experimental results

The mass spectrum resulting from the photodissociation of $CdH_2^+HSO_4^-$ at 266 nm is shown in **Figure 10**, as well as its CID spectrum. The conditions (collision voltage or UV power) have been adjusted so that the total fragmentation yield is the same for the two spectra, namely, 0.33, which allows better comparison between them. The UVPD spectrum is noisier because light scattered from the laser may create stray ions, but the two spectra show identical fragmentation

pattern, with the major fragment being the protonated monomer. In contrast with CdH^+ itself, the CdH_2^{2+}:HSO_4^- complex (*m/z* 393) does not show any specific UVPD photo-fragment, and the same behavior is observed for Qn or Qd. **Figure 10** also shows the CID spectrum of CdH^+ (*m/z* 295) produced by UV irradiation of the complex. The fragmentation pattern is the same as observed for CdH^+ formed in the ESI, with the main channels being water loss (*m/z* 277) or loss of water and methylamine (*m/z* 246). The fragmentation efficiency for a given radiofrequency amplitude is of the same order as that of CdH^+ formed in the ESI.[54]

2.2. Excited states calculations

Vertical excitation energies and nature of the first three excited states: The energies of the first three vertical electronic transitions of Syn-γ-closed' are listed in **Table 7**. We have limited the table to the transitions below the energy of the UV laser (4.66 eV). Table 7 also includes the doubly protonated monomer $CdH_2^{2+}$for the sake of comparison. However, this doubly charged species is not stable in the gas phase and was not observed in our experimental conditions. Therefore, its PES was not fully explored. The structure of isolated CdH_2^{2+} presented in the table is a local minimum obtained by optimizing the geometry of CdH_2^{2+}, starting from the geometry contained in the CdH_2^{2+}:HSO_4^- Syn-γ-closed' complex. Finally, the table includes the results for the corresponding monomers protonated on N_{alk} or $CdN_{arom}H^+$, the corresponding monomer protonated on N_{arom}, in the same geometry as contained in the complex. In short, the systems will be denoted by CdH_2^{2+}:HSO_4^-, CdH_2^{2+}, CdH^+, and $CdN_{arom}H^+$ in what follows. **Figure 11** shows the difference between the electronic density of the ground state and that of the first three excited states of CdH^+, $CdN_{arom}H^+$, CdH_2^{2+} and CdH_2^{2+}:HSO_4^-. In the discussion that follows, the canonical occupied HF orbitals delocalized all over the two aromatic rings will be denoted by π_{arom} and the unoccupied one by π^*_{arom}, while the occupied orbitals localized on the aza C_6 ring or carbonaceous C_6 ring will be denoted by π_{aromN} or π_{aromC}, respectively. Similarly, the unoccupied ones will be denoted by π^*_{aromN} or π^*_{aromC} respectively. The N_{akl} and N_{arom} lone pairs will be denoted by n_{Nalk} and n_{Narom}, respectively. Finally, the canonical HF orbitals localized on the alkaloid C=C group will be denoted by π_{CC} or π^*_{CC}, respectively.

The three lower-energy transitions of CdH^+ involve aromatic π electrons as well as the lone pair located on N_{arom}, as suggested for quinoline (**Figure 11a**).[100] The $S_{1\leftarrow0}$ transition mainly involves HOMO-4 (mostly N_{arom} lone pair) → LUMO (π^*_{arom}) (68%) and HOMO-3 (mixed N_{arom} lone pair and π_{arom}) → LUMO (24 %) excitations. It is therefore an intramolecular charge transfer (CT) within the aromatic ring, i.e. a $n_{arom}\pi^*_{arom}$ CT transition. The $S_{2\leftarrow0}$ and $S_{3\leftarrow0}$ electronic

transitions are ππ* transitions localized on the aromatic ring. They involve the very same orbitals HOMO-1(π_{arom})→ LUMO (64%) and HOMO (π_{arom}) → LUMO+1 (π^*_{arom}) (30%) for $S_{2\leftarrow0}$ and HOMO-1 →LUMO (85%) for $S_{3\leftarrow0}$ as the so-called L_b and L_a electronic transitions of naphthalene derivatives.[101 102 68]

In $CdN_{arom}H^+$, (**Figure 11b**), the $S_{1\leftarrow0}$ transition mainly involves HOMO (mostly n_{Nalk}) → LUMO (mostly π^*_{arom}) (40%) and HOMO-1 (n_{Nalk} and π_{aromC}) → LUMO (37 %) excitations. The $S_{1\leftarrow0}$ transition is therefore mainly an intramolecular charge transfer from n_{Nalk} to π^*_{arom}, *i.e.* a $n_{alk}\pi^*_{arom}$ CT transition. The $S_{2\leftarrow0}$ transition is mainly a naphthalene-like $\pi_{arom}\pi^*_{arom}$ transition that involves HOMO-2 (π_{arom}) → LUMO (54%) and HOMO-1 → LUMO (31%) excitations. Finally, the $S_{3\leftarrow0}$ transition involves HOMO-1 → LUMO+1 (π^*_{arom}) (44%) and HOMO → LUMO+1 (35%) excitations, it is mainly a naphthalene-like $\pi_{arom}\pi^*_{arom}$ transition.

For CdH_2^{2+}, (**Figure 11c**), both nitrogen atoms are protonated and there is no possibility for CT nπ* transitions involving a nitrogen lone pair. The $S_{1\leftarrow0}$ and $S_{2\leftarrow0}$ transitions are of ππ* character. $S_{1\leftarrow0}$ corresponds to the HOMO-1 (π_{aromC}) → LUMO (π^*_{arom}) (94%) excitation, while $S_{2\leftarrow0}$ corresponds to HOMO-2 (π_{arom}) → LUMO (72%) and HOMO-1→LUMO+1 (π_{arom}) (26%), respectively. Interestingly, the $S_{3\leftarrow0}$ transition corresponds to an intramolecular charge-transfer from the alkaloid C=C to the aromatic ring. Indeed, it is a HOMO → LUMO transition (95%) with the HOMO orbital being the $\pi_{C=C}$ orbital of the C=C double bond.

In the CdH_2^{2+}:HSO_4^- complex also, both nitrogen atoms of CdH_2^{2+} are protonated and there is no possibility for intramolecular CT involving a nitrogen lone pair (**Figure 11d**). The presence of HSO_4^- completely modifies the nature of the $S_{1\leftarrow0}$ transition compared to CdH_2^{2+}. At equilibrium distance, the charge transfer transition involving the $\pi_{C=C}$ orbital is out of the manifold of the transitions reached by the UV laser. The $\pi_{C=C}$ orbital corresponds to the HOMO and is involved in none of the first five electronic transitions, and only marginally in $S_{6\leftarrow0}$, which is higher in energy (5.23 eV) than the laser energy. $S_{1\leftarrow0}$ now corresponds to HOMO-3 → LUMO excitation (93%), with the HOMO-3 being mainly described in terms of combination of the lone pairs n_O of the oxygen atoms of the three S=O groups of HSO_4^-, and the LUMO being a π^*_{aromN} orbital. The $S_{1\leftarrow0}$ transition can therefore be described in terms of a $n_O\pi^*_{aromN}$ intermolecular CT from the bisulfate to CdH_2^{2+}. The $S_{2\leftarrow0}$ and $S_{3\leftarrow0}$ transitions correspond to HOMO-1(π_{aromC}) → LUMO (81%) and to HOMO-2 (π_{arom}) → LUMO, (61%), respectively. They are of ππ* nature.

Modification of the electronic transitions when elongating the NH bonds:

Based on calculations of the excited states at the same level as in this work, it was proposed previously that the photoreactivity of the closed forms of CdH^+ arises from proton transfer from N_{alk} to N_{arom}. The $CdN_{arom}H^+$ formed thereby undergoes electron transfer from the C=C group of the alkaloid to N_{arom}, resulting to the formation of specific photofragments.[53] This was confirmed by the experimental finding that in a similar system, hydroquinine, in which the CC bond is saturated, there is no formation of photofragments.[53] Elongating the $N_{arom}H^+$ bond in $CdN_{arom}H^+$ lowers the charge-transfer transition that plays a major role in the reactivity of the cinchona alkaloids, like the charge transfer involving CO in tyrosine containing peptides.[38 53] We have therefore calculated the change in electron density for the first three electronic transitions of CdH_2^{2+} and CdH_2^{2+}:HSO_4^-, when elongating either the $N_{alk}H$ or the $N_{arom}H$ distances. The density difference between the ground state and the first three excited states of the complex is compared to that in CdH_2^{2+}in **Figure 12**. In CdH_2^{2+}, the $S_{1\leftarrow0}$ transition for the $N_{alk}H^+$ bond modified from its equilibrium distance (1.023 Å) to 2.000 Å is an intramolecular charge transfer within the alkaloid part of the molecule. It is mostly a HOMO ($\pi_{C=C}$) → LUMO ($\sigma^*_{NalkH^+}$) (96%) transition. It is therefore a CT transition from the $\pi_{C=C}$ orbital to the $\sigma^*_{NalkH^+}$ orbital.[53] For the $N_{arom}H^+$ bond elongated from its equilibrium distance (1.018 Å) to 2.000 Å the $S_{1\leftarrow0}$ and $S_{2\leftarrow0}$ are HOMO-1 (π_{arom}) → LUMO ($\sigma^*_{NaromH^+}$) (96%) and HOMO-2 (π_{arom}) → LUMO ($\sigma^*_{NaromH^+}$) (98%) transitions. However, the $S_{3\leftarrow0}$ transition is a HOMO ($\pi_{C=C}$) → LUMO (97%) transition, *i.e.* a charge transfer from the C=C group localized on the alcaloid. In both cases, one of the first three electronic transitions, namely, $S_{1\leftarrow0}$ when elongating the $N_{alk}H^+$ bond or $S_{3\leftarrow0}$, when elongating the $N_{arom}H^+$ bond involves charge migration from the $\pi_{C=C}$ orbital to the $\sigma^*_{NH^+}$.

The CdH_2^{2+}:HSO_4^- complex behaves differently from CdH_2^{2+}. Elongating the $N_{alk}H^+$ bond from its equilibrium distance is prevented by the cage effect due to the presence of HSO_4^-. Elongating the $N_{arom}H$ bond from its equilibrium value (1.017Å) to 2.000 Å has two consequences. Compared to CdH_2^{2+}, it modifies the energy order of the transition. For an identical $N_{arom}H$ distance, of 2.000 Å, $S_{2\leftarrow0}$ and $S_{3\leftarrow0}$ in the complex are similar to $S_{2\leftarrow0}$ and $S_{1\leftarrow0}$ in CdH_2^{2+}, respectively in terms of excitations type and then electron density changes. $S_{1\leftarrow0}$ in the complex is the HOMO-3 → LUMO excitation (90%), with the HOMO-3 being mainly described in terms of combination of the n_O of the three S=O groups of HSO_4^-, and the LUMO being the σ_{NaromH^+} orbital. It corresponds therefore to an intermolecular CT transition.

We can conclude from these results that the bisulfate anion has a protective effect and prevents photodissociation of the CdH_2^{2+}:HSO_4^- complex in two manners. Firstly, the fact that the two

nitrogen atoms, N_{alk} and N_{arom}, are protonated prevents proton transfer from N_{alk} to N_{arom}. Moreover, the short hydrogen bond between the bisulfate and N_{alk} induces a cage effect that prevents motions of the $N_{alk}H^+$. The second effect of the complex formation is that the CT transitions from the $\pi_{C=C}$ orbital of the alkaloid part of the molecule to the $\sigma^*_{NalkH^+}$ or σ_{NaromH^+} orbital are removed from the manifold accessible by the laser. Instead, the first three $S_{n\leftarrow 0}$ transition involve $\pi\pi^*$ excitations and then electron density changes within the quinoline ring, or charge migration from the bisulfate anion to the aza C_6 ring, or to the $\sigma^*_{NaromH^+}$.

Conclusion

This study unambiguously shows that the complexes formed between protonated cinchonidine and sulfuric acid actually contains doubly protonated cinchonidine CdH_2^{2+} and the bisulfate anion, HSO_4^-. The cinchona alkaloid is therefore protonated on both nitrogens, the alkaloid nitrogen N_{alk} and the aromatic nitrogen N_{arom}. HSO_4^- bridges the two protonation sites so that electrostatic interactions between CdH_2^{2+} and HSO_4^- stabilize the doubly protonated species in the gas phase. The same structure as for cinchonidine is observed for quinine and quinidine. No chirality effect is observed in the structure of the complex.

The presence of bisulfate has several consequences on the photophysics of protonated cinchonidine. First, the cinchonidine contained in the complex is doubly protonated, so that the transitions involving the N_{alk} or N_{arom} lone pair are removed from the manifold. The presence of HSO_4^- also has a protective role towards photo-dissociation. It first prevents the mobility of the proton localized on N_{alk} thanks to the strong electrostatic interaction. Such a cage effect has already been observed in tryptamine, tryptophan, or cinchonidine itself, embedded in cyclodextrine.[53, 103, 104] This explains why the reactivity related to proton mobility, previously proposed for isolated CdH^+, is not observed here.[53] The second role of the bisulfate is to modify the nature of the electronic transitions. In particular, the CT transitions from $\pi_{C=C}$ orbital to $\sigma^*_{NalkH^+}$ or $\sigma^*_{NaromH^+}$, which has been supposed to play a role in the photodissociation of CdH^+, is higher than the laser energy in the complex.[53] This study emphasizes the role of counterions in protecting biomolecules from photodissociation. The influence of complexation by sulfuric acid on the protonated cinchona alkaloid dimers is currently in progress and will be reported in a near future.

Acknowledgment

We thank Dr J. M. Ortega and the CLIO team for technical assistance. We acknowledge the use of the computing center MésoLUM of the LUMAT research federation (FR LUMAT 2764).

The research described here has been supported by the Investissements d'Avenir LabEx PALM contract (ANR-10-LABX-0039-PALM), by the ANR contract (ESBODYR ANR-14-CE06-0019-03), and by the RTRA "Triangle de la Physique" contract (Project N°2013-0562-T, Chiraux IRUV). We thank Fabrice Gobert for experimental help. FB gratefully acknowledges the support of COST Action CM1405 (MOLIM).

References

1. M. Ichihashi, M. Ueda, A. Budiyanto, T. Bito, M. Oka, M. Fukunaga, K. Tsuru and T. Horikawa, *Toxicology*, 2003, **189**, 21-39.
2. J. Cadet, E. Sage and T. Douki, *Mutation Research-Fundamental and Molecular Mechanisms of Mutagenesis*, 2005, **571**, 3-17.
3. R. P. Sinha and D. P. Hader, *Photochemical & Photobiological Sciences*, 2002, **1**, 225-236.
4. H. H. Tonnesen, *International Journal of Pharmaceutics*, 2001, **225**, 1-14.
5. G. Cosa, K. S. Focsaneanu, J. R. N. McLean, J. P. McNamee and J. C. Scaiano, *Photochemistry and Photobiology*, 2001, **73**, 585-599.
6. J. M. L. Pecourt, J. Peon and B. Kohler, *Journal of the American Chemical Society*, 2001, **123**, 10370-10378.
7. C. E. Crespo-Hernandez, B. Cohen, P. M. Hare and B. Kohler, *Chemical Reviews*, 2004, **104**, 1977-2019.
8. C. T. Middleton, K. de La Harpe, C. Su, Y. K. Law, C. E. Crespo-Hernandez and B. Kohler, in *Annu. Rev. Phys. Chem.*, 2009, vol. 60, pp. 217-239.
9. D. Onidas, D. Markovitsi, S. Marguet, A. Sharonov and T. Gustavsson, *Journal of Physical Chemistry B*, 2002, **106**, 11367-11374.
10. T. Gustavsson, A. Banyasz, E. Lazzarotto, D. Markovitsi, G. Scalmani, M. J. Frisch, V. Barone and R. Improta, *Journal of the American Chemical Society*, 2006, **128**, 607-619.
11. C. Canuel, M. Mons, F. Piuzzi, B. Tardivel, I. Dimicoli and M. Elhanine, *Journal of Chemical Physics*, 2005, **122**.
12. S. Ullrich, T. Schultz, M. Z. Zgierski and A. Stolow, *Physical Chemistry Chemical Physics*, 2004, **6**, 2796-2801.
13. H. Kang, K. T. Lee, B. Jung, Y. J. Ko and S. K. Kim, *Journal of the American Chemical Society*, 2002, **124**, 12958-12959.
14. B. Lucas, M. Barat, J. A. Fayeton, M. Perot, C. Jouvet, G. Gregoire and S. B. Nielsen, *Journal of Chemical Physics*, 2008, **128**, 164302.
15. L. Joly, R. Antoine, M. Broyer, P. Dugourd and J. Lemoine, *Journal of Mass Spectrometry*, 2007, **42**, 818-824.
16. J. P. Reilly, *Mass Spectrometry Reviews*, 2009, **28**, 425-447.
17. J. P. O'Brien and J. S. Brodbelt, *Analytical Chemistry*, 2013, **85**, 10399-10407.
18. C. Y. Lin and R. C. Dunbar, *Journal of Physical Chemistry*, 1995, **99**, 1754-1759.
19. Z. Q. Guan, N. L. Kelleher, P. B. Oconnor, D. J. Aaserud, D. P. Little and F. W. McLafferty, *International Journal of Mass Spectrometry and Ion Processes*, 1996, **157**, 357-364.
20. J. H. Moon, Y. S. Shin, H. J. Cha and M. S. Kim, *Rapid Communications in Mass Spectrometry*, 2007, **21**, 359-368.
21. N. C. Polfer, *Chem. Soc. Rev.*, 2011, **40**, 2211-2221.
22. A. M. Rijs and J. Oomens, eds., *Gas-Phase IR Spectroscopy and Structure of Biological Molecules*, Springer International Publishing, 2015.

23. I. Alata, J. Bert, M. Broquier, C. Dedonder, G. Feraud, G. Gregoire, S. Soorkia, E. Marceca and C. Jouvet, *Journal of Physical Chemistry A*, 2013, **117**, 4420-4427.
24. I. Alata, M. Broquier, C. Dedonder, C. Jouvet and E. Marceca, *Chemical Physics*, 2012, **393**, 25-31.
25. S. Daly, M. Krstic, A. Giuliani, R. Antoine, L. Nahon, A. Zavras, G. N. Khairallah, V. Bonacic-Koutecky, P. Dugourd and R. A. J. O'Hair, *Physical Chemistry Chemical Physics*, 2015, **17**, 25772-25777.
26. J. A. Madsen, D. R. Boutz and J. S. Brodbelt, *Journal of Proteome Research*, 2010, **9**, 4205-4214.
27. L. Joly, R. Antoine, A. R. Allouche and P. Dugourd, *Journal of the American Chemical Society*, 2008, **130**, 13832-13833.
28. F. O. Talbot, T. Tabarin, R. Antoine, M. Broyer and P. Dugourd, *Journal of Chemical Physics*, 2005, **122**.
29. C. S. Hansen, S. J. Blanksby, N. Chalyavi, E. J. Bieske, J. R. Reimers and A. J. Trevitt, *Journal of Chemical Physics*, 2015, **142**.
30. C. S. Hansen, S. J. Blanksby and A. J. Trevitt, *Phys. Chem. Chem. Phys.*, 2015, DOI: DOI: 10.1039/C5CP02035B.
31. K. Ranka, N. Zhao, L. Yu, J. F. Stanton and N. C. Polfer, *Journal of the American Society for Mass Spectrometry*, 2018, **29**, 1791-1801.
32. Y. Inokuchi, R. Kusaka, T. Ebata, O. V. Boyarkin and T. R. Rizzo, *Chemphyschem*, 2013, **14**, 649-660.
33. T. N. Wassermann, O. V. Boyarkin, B. Paizs and T. R. Rizzo, *Journal of the American Society for Mass Spectrometry*, 2012, **23**, 1029-1045.
34. A. Kamariotis, O. V. Boyarkin, S. R. Mercier, R. D. Beck, M. F. Bush, E. R. Williams and T. R. Rizzo, *Journal of the American Chemical Society*, 2006, **128**, 905-916.
35. G. Feraud, M. Broquier, C. Dedonder, C. Jouvet, G. Gregoire and S. Soorkia, *The Journal of Physical Chemistry A*, 2015, **119**, 5914-5924.
36. H. Kang, G. Feraud, C. Dedonder-Lardeux and C. Jouvet, *Journal of Physical Chemistry Letters*, 2014, **5**, 2760-2764.
37. G. Feraud, M. Broquier, C. Dedonder-Lardeux, G. Gregoire, S. Soorkia and C. Jouvet, *Physical Chemistry Chemical Physics*, 2014, **16**, 5250-5259.
38. C. Dehon, S. Soorkia, M. Pedrazzani, C. Jouvet, M. Barat, J. A. Fayeton and B. Lucas, *Physical Chemistry Chemical Physics*, 2013, **15**, 8779-8788.
39. A. B. Wolk, C. M. Leavitt, E. Garand and M. A. Johnson, *Accounts of Chemical Research*, 2014, **47**, 202-210.
40. C. M. Choi, D. H. Choi, N. J. Kim and J. Heo, *International Journal of Mass Spectrometry*, 2012, **314**, 18-21.
41. G. A. Pino, G. Feraud, M. Broquier, G. Gregoire, S. Soorkia, C. Dedonder and C. Jouvet, *Physical Chemistry Chemical Physics*, 2016, **18**, 20126-20134.
42. M. Broquier, S. Soorkia, C. Dedonder-Lardeux, C. Jouvet, P. Theule and G. Gregoire, *Journal of Physical Chemistry A*, 2016, **120**, 3797-3809.
43. M. Lammerhofer and W. Lindner, *Journal of Chromatography A*, 1996, **741**, 33-48.
44. O. J. Sonderegger, G. M. W. Ho, T. Burgi and A. Baiker, *Journal of Catalysis*, 2005, **230**, 499-506.
45. C. E. Song, *Cinchona Alkaloids in Synthesis and Catalysis*, Wiley-VCH, Weinheim, 2009.
46. T. Burgi and A. Baiker, *Accounts of Chemical Research*, 2004, **37**, 909-917.
47. J. Wang, L. D. Heikkinen, H. Li, L. S. Zu, W. Jiang, H. X. Xie and W. Wang, *Advanced Synthesis & Catalysis*, 2007, **349**, 1052-1056.
48. A. Adili, Z. L. Tao, D. F. Chen and Z. Y. Han, *Organic & Biomolecular Chemistry*, 2015, **13**, 2247-2250.
49. B. L. Diffey, P. M. Farr and S. J. Adams, *British Journal of Dermatology*, 1988, **118**, 679-685.
50. W. W. Qin, A. Vozza and A. M. Brouwer, *Journal of Physical Chemistry C*, 2009, **113**, 11790-11795.
51. J. Qian and A. M. Brouwer, *Physical Chemistry Chemical Physics*, 2010, **12**, 12562-12569.
52. W. H. Melhuish, *Journal of Physical Chemistry*, 1961, **65**, 229-&.
53. S. Kumar, B. Lucas, J. Fayeton, D. Scuderi, I. Alata, M. Broquier, K. Le Barbu-Debus, V. Lepere and A. Zehnacker, *Physical Chemistry Chemical Physics*, 2016, **18**, 22668-22677.

54. I. Alata, D. Scuderi, V. Lepere, V. Steinmetz, F. Gobert, L. Thiao-Layel, K. Le Barbu-Debus and A. Zehnacker-Rentien, *Journal of Physical Chemistry A*, 2015, **119**, 10007-10015.
55. A. Zehnacker, *International Reviews in Physical Chemistry*, 2014, **33**, 151-207.
56. D. Scuderi, K. Le Barbu-Debus and A. Zehnacker, *Physical Chemistry Chemical Physics*, 2011, **13**, 17916-17929.
57. D. Scuderi, P. Maitre, F. Rondino, K. Le Barbu-Debus, V. Lepere and A. Zehnacker-Rentien, *Journal of Physical Chemistry A*, 2010, **114**, 3306-3312.
58. D. Scuderi, V. Lepere, G. Piani, A. Bouchet and A. Zehnacker-Rentien, *Journal of Physical Chemistry Letters*, 2014, **5**, 56.
59. P. E. Hintze, H. G. Kjaergaard, V. Vaida and J. B. Burkholder, *Journal of Physical Chemistry A*, 2003, **107**, 1112-1118.
60. P. E. Hintze, K. J. Feierabend, D. K. Havey and V. Vaida, *Spectrochimica Acta Part a-Molecular and Biomolecular Spectroscopy*, 2005, **61**, 559-566.
61. M. Rozenberg, A. Loewenschuss and C. J. Nielsen, *Journal of Physical Chemistry A*, 2011, **115**, 5759-5766.
62. L. Mac Aleese, A. Simon, T. B. McMahon, J.-M. Ortega, D. Scuderi, J. Lemaire and P. Maître, *International Journal of Mass Spectrometry*, 2006, **249-250**, 14-20.
63. J. B. Fenn, M. Mann, C. K. Meng, S. F. Wong and C. M. Whitehouse, *Science. 1989 Oct 6;246(4926):64-71.*, 1989.
64. R. Prazeres, J. M. Berset, F. Glotin, D. Jaroszynski and J. M. Ortega, *Nuclear Instruments & Methods in Physics Research Section a-Accelerators Spectrometers Detectors and Associated Equipment*, 1993, **331**, 15-19.
65. *MacroModel version 9.8; ed. Schrödinger, LLC: New York, NY, 2010*, 2010.
66. E. Harder, W. Damm, J. Maple, C. Wu, M. Reboul, J. Y. Xiang, L. Wang, D. Lupyan, M. K. Dahlgren, J. L. Knight, J. W. Kaus, D. S. Cerutti, G. Krilov, W. L. Jorgensen, R. Abel and R. A. Friesner, *Journal of Chemical Theory and Computation*, 2016, **12**, 281-296.
67. H. T. A., *Journal of Computational Chemistry*, 1999, **20**, 720-729.
68. A. Sen, A. Bouchet, V. Lepere, K. Le Barbu-Debus, D. Scuderi, F. Piuzzi and A. Zehnacker-Rentien, *The Journal of Physical Chemistry. A*, 2012, **116**, 8334-8344.
69. L. Goerigk and S. Grimme, *Physical Chemistry Chemical Physics*, 2011, **13**, 6670-6688.
70. S. Grimme, J. Antony, S. Ehrlich and H. Krieg, *Journal of Chemical Physics*, 2010, **132**.
71. A. D. Becke, *Physical Review A*, 1988, **38**, 3098-3100.
72. M. D. Halls, J. Velkovski and H. B. Schlegel, *Theoretical Chemistry Accounts*, 2001, **105**, 413.
73. M. J. Frisch, J. A. Pople and J. S. Binkley, *Journal of Chemical Physics*, 1984, **80**, 3265-3269.
74. S. Grimme, S. Ehrlich and L. Goerigk, *Journal of Computational Chemistry*, 2011, **32**, 1456-1465.
75. J. Altnoeder, A. Bouchet, J. J. Lee, K. E. Otto, M. A. Suhm and A. Zehnacker-Rentien, *Physical Chemistry Chemical Physics*, 2013, **15**, 10167-10180.
76. S. Boys and F. Bernardi, *Mol. Phys.*, 1970, **19**, 553.
77. T. Troxler, B. A. Pryor and M. R. Topp, *Chem. Phys. Lett.*, 1997, **274**, 71-78.
78. M. J. Frisch, G. W. Trucks, H. B. Schlegel, G. E. Scuseria, M. A. Robb, J. R. Cheeseman, J. A. Montgomery, T. V. Jr., K. N. Kudin, J. C. Burant, J. M. Millam, S. S. Iyengar, J. Tomasi, V. Barone, B. Mennucci, M. Cossi, G. Scalmani, N. Rega, G. A. Petersson, H. Nakatsuji, M. Hada, M. Ehara, K. Toyota, R. Fukuda, J. Hasegawa, M. Ishida, T. Nakajima, Y. Honda, O. Kitao, H. Nakai, M. Klene, X. Li, J. E. Knox, H. P. Hratchian, J. B. Cross, V. Bakken, C. Adamo, J. Jaramillo, R. Gomperts, R. E. Stratmann, O. Yazyev, A. J. Austin, R. Cammi, C. Pomelli, J. W. Ochterski, P. Y. Ayala, K. Morokuma, G. A. Voth, P. Salvador, J. J. Dannenberg, V. G. Zakrzewski, S. Dapprich, A. D. Daniels, M. C. Strain, O. Farkas, D. K. Malick, A. D. Rabuck, K. Raghavachari, J. B. Foresman, J. V. Ortiz, Q. Cui, A. G. Baboul, S. Clifford, J. Cioslowski, B. B. Stefanov, G. Liu, A. Liashenko, P. Piskorz, I. Komaromi, R. L. Martin, D. J. Fox, T. Keith, M. A. Al-Laham, C. Y. Peng, A. Nanayakkara, M. Challacombe, P. M. W. Gill, B. Johnson, W. Chen, M. W. Wong, C. Gonzalez and J. A. Pople, *Journal*, 2004.
79. A. R. Allouche, *Journal of Computational Chemistry*, 2011, **32**, 174.
80. C. Hattig and F. Weigend, *Journal of Chemical Physics*, 2000, **113**, 5154-5161.

81. F. Weigend and M. Haser, *Theoretical Chemistry Accounts*, 1997, **97**, 331-340.
82. T. H. Dunning, *Journal of Chemical Physics*, 1989, **90**, 1007-1023.
83. R. L. Garcia, N. Nieuwjaer, C. Desfrancois, F. Lecomte, S. D. Leite, B. Manil, M. Broquier and G. Gregoire, *Physical Chemistry Chemical Physics*, 2017, **19**, 8258-8268.
84. R. Ahlrichs, M. Bar, M. Haser, H. Horn and C. Kolmel, *Chemical Physics Letters* 1989, **162**, 165-169.
85. W. Humphrey, A. Dalke and K. Schulten, *J. Molec. Graphics*, 1996, **14**, 33-38.
86. A. Givan, L. A. Larsen, A. Loewenschuss and C. J. Nielsen, *Journal of Molecular Structure*, 1999, **509**, 35-47.
87. http://cccbdb.nist.gov/vibscalejust.asp).
88. R. Paciotti, C. Coletti, N. Re, D. Scuderi, B. Chiavarino, S. Fornarini and M. E. Crestoni, *Physical Chemistry Chemical Physics*, 2015, **17**, 25891-25904.
89. L. Barnes, B. Schindler, A. R. Allouche, D. Simon, S. Chambert, J. Oomens and I. Compagnon, *Physical Chemistry Chemical Physics*, 2015, **17**, 25705-25713.
90. T. I. Yacovitch, T. Wende, L. Jiang, N. Heine, G. Meijer, D. M. Neumark and K. R. Asmis, *Journal of Physical Chemistry Letters*, 2011, **2**, 2135-2140.
91. J. J. Max, C. Menichelli and C. Chapados, *Journal of Physical Chemistry A*, 2000, **104**, 2845-2858.
92. C. Menichelli, J. J. Max and C. Chapados, *Canadian Journal of Chemistry-Revue Canadienne De Chimie*, 2000, **78**, 1128-1142.
93. K. L. Nash, K. J. Sully and A. B. Horn, *Physical Chemistry Chemical Physics*, 2000, **2**, 4933-4940.
94. A. Urakawa, D. M. Meier, H. Rugger and A. Baiker, *Journal of Physical Chemistry A*, 2008, **112**, 7250-7255.
95. T. Burgi and A. Baiker, *Journal of the American Chemical Society*, 1998, **120**, 12920-12926.
96. H. Caner, P. U. Biedermann and I. Agranat, *Chirality*, 2003, **15**, 637-645.
97. A. Sen, V. Lepere, K. Le Barbu-Debus and A. Zehnacker, *Chemphyschem : a European Journal of Chemical Physics and Physical Chemistry*, 2013, **14**, 3559-3568.
98. F. Lahmani, K. Le Barbu-Debus, N. Seurre and A. Zehnacker-Rentien, *Chem. Phys. Lett.*, 2003, **375**, 636-644.
99. L. Alvarez-Valtierra, J. W. Young and D. W. Pratt, *Chem. Phys. Lett.*, 2011, **509**, 96-101.
100. A. Hiraya, Y. Achiba, K. Kimura and E. C. Lim, *Journal of Chemical Physics*, 1984, **81**, 3345-3347.
101. S. M. Beck, D. E. Powers, J. B. Hopkins and R. E. Smalley, *Journal of Chemical Physics*, 1980, **73**, 2019.
102. F. Lahmani, E. Breheret, A. Zehnackerrentien and T. Ebata, *Journal of the Chemical Society-Faraday Transactions*, 1993, **89**, 623-629.
103. A. Fujihara, T. Sato and S. Hayakawa, *Chem. Phys. Lett.*, 2014, **610**, 228-233.
104. U. Kadhane, M. Perot, B. Lucas, M. Barat, J. A. Fayeton, C. Jouvet, A. Ehlerding, M. B. S. Kirketerp, S. B. Nielsen, J. A. Wyer and H. Zettergren, *Chem. Phys. Lett.*, 2009, **480**, 57-61.

Figures and Tables

Table1: Significant calculated dihedral angles (°) and distances (Å) of the most stable conformers of the $CdH^{+}H_2SO_4$ complex optimized at the B3LYP-D3/6-31++G(d,p) level.

Dihedral angles (°) and distances (Å)	**Anti-γ-open**	**Anti-γ-open'**	**Anti-γ-closed**	**Anti-γ-closed'**
τ_1 (C_3-C_4, C_9 C_8)	100	109	68	70
τ_2 (C_4, C_9 C_8 N_{alk})	168	164	44	54
τ_3 (N C_8 C_9 O)	-69	-71	165	175
T_3 (C_8 C_9 O H)	-179	172	172	179
$d_{N_{alk}H^{\delta+}...^{\delta-}OS}$	1.88	1.88	1.84	1.87
$d_{N_{arom}...HOS}$	7.14	5.47	1.58	3.38

Table 2: Significant calculated dihedral angles (°) and distances (Å) of the most stable conformers of the $CdH_2^{+}HSO_4^{-}$ complex optimized at the B3LYP-D3/6-31++G(d,p) level.

Dihedral angles (°) and distances (Å)	**Syn-γ-closed**	**Syn-γ-closed'**	**Anti-γ-closed**	**Anti-β-open**	**Syn-γ-open**
τ_1 (C_3-C_4-C_9 C_8)	-108	-107	68	100	-83
τ_2(C_4-$C_9$$C_8$ N_{alk})	72	47	58	165	161
τ_3 (N C_8 C_9 O)	-165	171	177	-71	-73
T_3 (C_8 C_9 O H)	172	165	169	108	149
$d_{N_{alk}H^{+\delta}...^{-\delta}OS}$	1.64	1.62	1.6	1.57	1.58
$d_{N_{arom}H^{+\delta}...^{-\delta}OS}$	2.76	2.35	2.66	7.03	6.17

Table 3: Calculated relative electronic energy **ΔE** and Gibbs free energy **ΔG** including counterpoise correction, for $CdH^{+}H_2SO_4$ and $CdH_2^{2+}HSO_4^{-}$ at the B3LYP-D3/ 6-31++G (d,p) level of theory. Counterpoise correction to the energy **BSSE**. Natural charges on significant atoms **q**. The notation used for for CdH^{+} and CdH^{2+} is taken from reference [55].

Molecules	ΔE (kcal/mol) with counterpoise correction	ΔG (kcal/mol) with counterpoise correction	BSSE (kcal/mol)	q(O) (…$N_{alk}H^+$)	q(O) (… N_{arom}^+)	q(O) (free)	q(H) ($N_{alk}H^+$)	q(H) ($N_{arom}H^+$)	q(S)	q(H) (SOH)	q(O) (SOH)
H_2SO_4	-	-	-	-	-	-0.90	-	-	2.53	0.53	-0.90
CdH^+ Anti γ-closed	-	-	-	-	-	-	0.48	-	-	-	-
$CdH^+H_2SO_4$											
Anti γ-open	17.5	14.5	2.2	-0.96	-	-0.88	0.49	-	2.57	0.55	-0.90
Anti γ-open'	16.7	16.2	2.3	-0.94	-	-0.91	0.49	-	2.56	0.55	-0.89
Anti γ-closed	8.0	7.5	3.0	-0.89	-	-1.01	0.51	-	2.59	0.54	-0.91
Anti γ-closed'	14.2	13.2	2.6	-0.94	-	-0.91	0.50	-	2.57	0.55	-0.89
HSO_4^-	-	-		-	-	-1.02 -1.02 -1.00	-	-	2.53	0.49	-0.97
CdH_2^{2+} Anti-γ-closed	-	-		-	-	-	0.47	0.48	-	-	-
$CdH_2^{2+}HSO_4^-$											
Anti-β-open	3.0	2.2	2.6	-1.01	-	-0.98 -1.03 *	0.51	0.46	2.56	0.53	-0.90

Syn-γ-open	5.0	4.8	2.3	-1.01	-	-1.03 *	0.51	0.46	2.56	0.53	-0.90
Syn-γ-closed'	0.1	0.0	2.7	-1.04	-0.99	-0.92	0.51	0.49	2.56	0.53	-0.92
Anti-γ-closed	0.5	0.4	2.7	-1.03	-0.99	-0.92	0.51	0.48	2.56	0.53	-0.92
Syn-γ-closed	0.0	0.2	2.7	-1.02	-0.99	-1.02	0.51	0.47	2.56	0.53	-0.92

* H bond acceptor from OH

Table 4: Significant calculated dihedral angles (°) and distances (Å) of the most stable conformers of the **Cis** $QnH_2^{2+}HSO_4^-$ complex optimized at the B3LYP-D3/6-31++G(d,p) level of theory.

Dihedral angles (°) and distances (Å)	**Cis-Anti-β-open**	**Cis-Syn-γ-open**	**Cis-Syn-γ-closed**	**Cis-Syn-γ-closed'**	**Cis-Anti-γ-closed**
τ_1 (C_3, C_4, C_9 C_8)	98	-85	-110	-107	74
τ_2 (C_4, $C_9C_8N_{alk}$)	162	160	59	47	60
τ_3 (N C_8 C_9 O)	-74	-73	-178	171	-180
T_3 (C_8 C_9 O H)	111	151	171	165	170
$d_{N_{alk}H^{+\delta}...^{-\delta}OS}$	1.6	1.58	1.62	1.62	1.64
$d_{N_{arom}H^{+\delta}...^{-\delta}OS}$	7.17	6.19	2.51	2.34	2.51

Table 5: Significant calculated dihedral angles (°) and distances (Å) of the most stable conformers of the **Trans** $QnH_2^{2+}HSO_4^-$ complex optimized at the B3LYP-D3/6-31++G(d,p) level of theory.

Dihedral angles (°) and distances (Å)	**Trans-Anti-β-open**	**Trans-Syn-γ-open**	**Trans-Syn-γ-closed**	**Trans-Syn-γ-closed'**	**Trans-Anti-γ-closed**
τ_1 (C_3, C_4, C_9 C_8)	103	-87	-109	-108	76
τ_2 (C_4, C_9 C_8N_{alk})	166	160	57	46	60
τ_3 (N C_8 C_9 O)	-71	-74	-180	170	180
T_3 (C_8 C_9 O H)	106	153	171	166	169
$d_{N_{alk}H^{+\delta}...^{-\delta}OS}$	1.57	1.58	1.62	1.63	1.67
$d_{N_{arom}H^{+\delta}...^{-\delta}OS}$	7.08	6.16	2.49	2.34	2.5

Table 6: Calculated relative electronic energy **ΔE** and Gibbs free energy **ΔG** including counterpoise correction, for the most stable conformers of $QnH_2^{2+}HSO_4^-$ at the B3LYP-D3/ 6-31++G (d,p) level of theory. Counterpoise correction to the energy **BSSE**.

Complex [$QnH_2^+HSO_4^-$]	**ΔE (kcal/mol)** with counterpoise correction	**ΔG (kcal/mol)** with counterpoise correction	**BSSE (kcal/mol)**
Cis-Anti-β-open	0.4	0.0	2.7
Cis-Syn-γ-open	5.9	5.0	2.3
Cis-Syn-γ-closed	0.0	0.6	3.0
Cis-Syn-γ-closed'	1.1	0.8	2.7
Cis-Anti-γ-closed	1.5	0.9	2.9
Trans-Anti-β-open	5.4	4	2.6
Trans-Syn-γ-open	7.1	5.9	2.3
Trans-Syn-γ-closed	1.2	1.7	2.9
Trans-Syn-γ-closed'	1.9	1.5	2.7
Trans-Anti-γ-closed	1.4	1.2	2.9

Table 7: Energy $\Delta E_{0\text{-}1,2,3}$ (eV) of the first three vertical transitions $S_{1,2,3\leftarrow 0}$ of the protonated monomer CdH^+, of the di-protonated monomer CdH_2^+ (see text), and of the $CdH_2^+HSO_4^-$ complex to which the experimental spectra has been assigned, all in the Syn-γ-closed conformation. The transition energy is given relative to the ground state of the corresponding system. Only the transitions below the laser energy (4.66 eV) are considered.

Protonated system	$\Delta E_{0\text{-}1}$	Orbitals involved in $S_{1\leftarrow 0}$	$\Delta E_{0\text{-}2}$	Orbitals involved in $S_{2\leftarrow 0}$	$\Delta E_{0\text{-}3}$	Orbitals involved in $S_{3\leftarrow 0}$
CdH^+	4.24	HOMO-4 →LUMO (68%) HOMO-3 →LUMO (24 %)	4.36	HOMO-1→LUMO (64%) HOMO→LUMO+1 (30%)	4.69	HOMO-1→LUMO (85%)
Cd $N_{arom}H^+$	2.48	HOMO→LUMO (40%) HOMO-1→LUMO (39%) HOMO-2 →LUMO (15%)	3.98	HOMO-2→LUMO (54%) HOMO-1→LUMO (31%)	4.09	HOMO→LUMO+1 (44%) HOMO-1→LUMO+1 (35%)
CdH_2^+	3.85	HOMO-1→LUMO (94%)	4.29	HOMO-2→LUMO (72%) HOMO-1→LUMO+1 (26%)	4.63	HOMO→LUMO (95%)
$CdH_2^+HSO_4^-$	3.80	HOMO-3→LUMO (93%)	4.09	HOMO-1→LUMO (81%)	4.17	HOMO-2 →LUMO (61%)

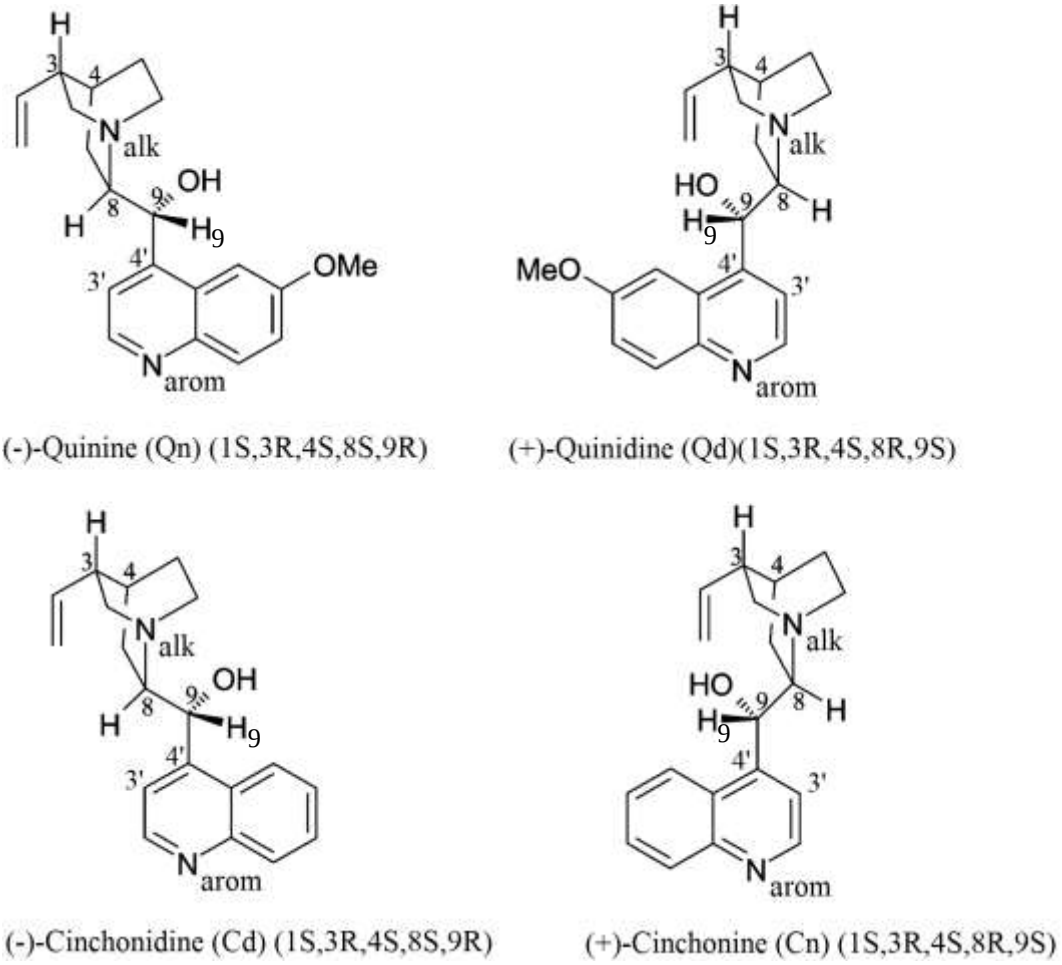

Figure 1: Structure of the molecules under study

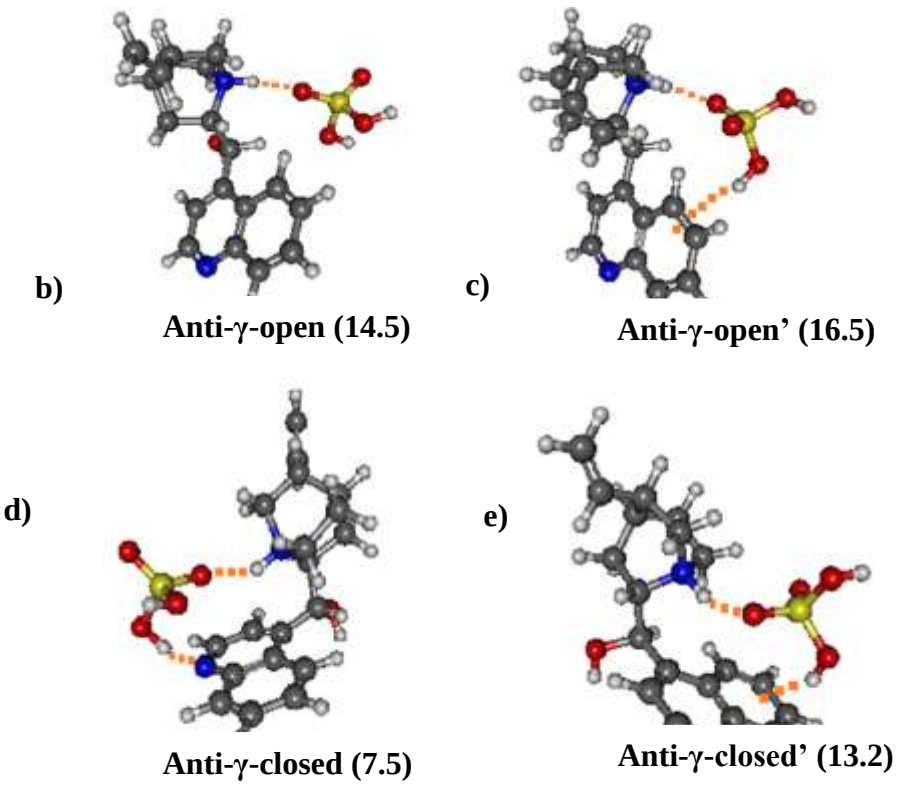

Figure 2: Structure of the four most stable conformers of the $CdH^{+}H_2SO_4$ complex calculated at the B3LYP-D3/6-31++G (d,p) level of theory. The Gibbs free energy relative to the most stable calculated complex is given in parentheses in kcal/mol

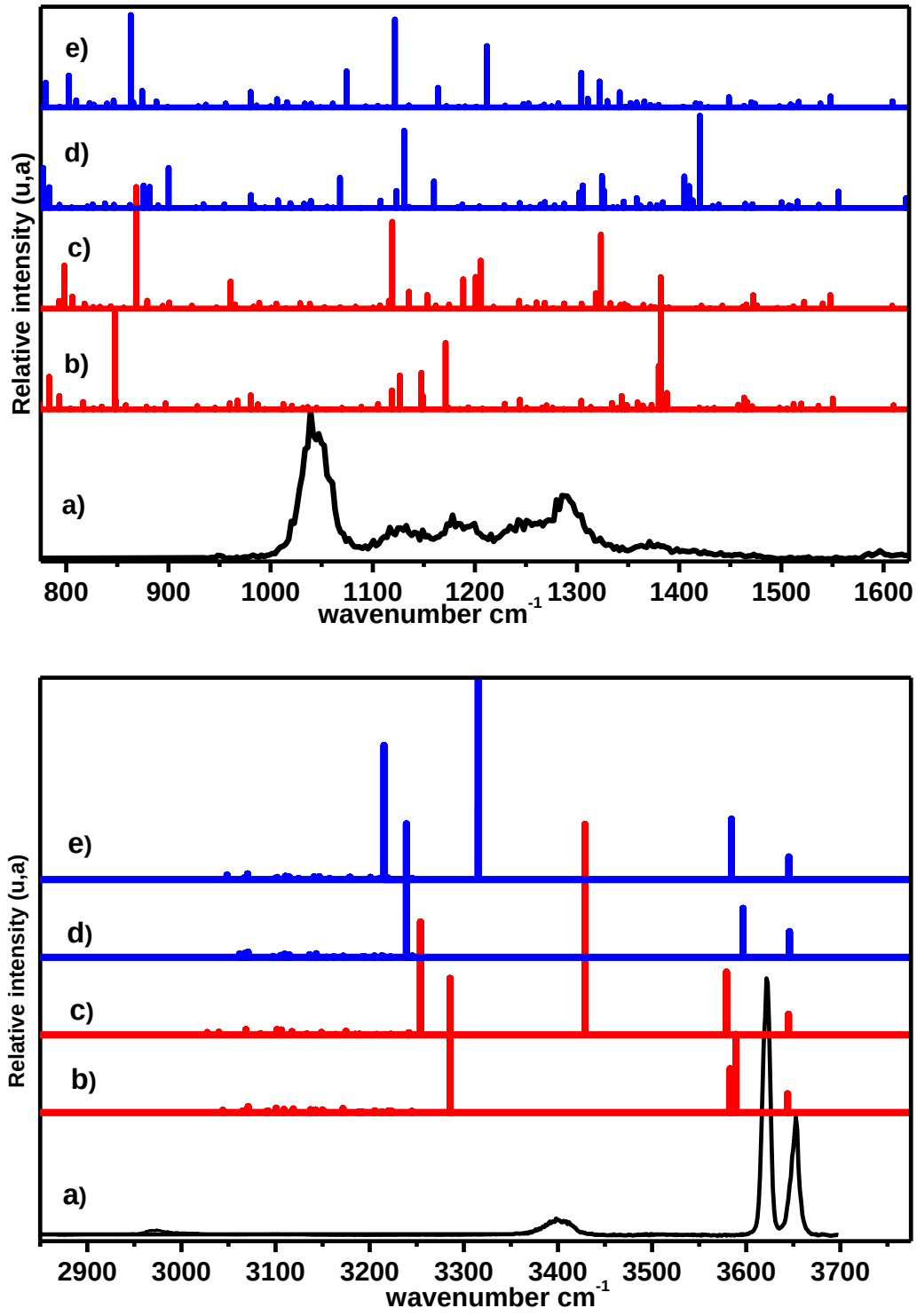

Figure 3: Comparison between the IR experimental spectrum of $CdH^+H_2SO_4$ (a) and the IR simulated spectra of the four most stable conformers: b) Anti-γ-open (Figure 2b), c) Anti-γ-open' (Figure 2c), d) Anti-γ-closed (Figure 2d), e) Anti-γ-closed' (Figure 2e). The spectra of the open conformers are in red and those of the closed conformers in blue. Fingerprint region (Top) and high frequency region (Bottom).

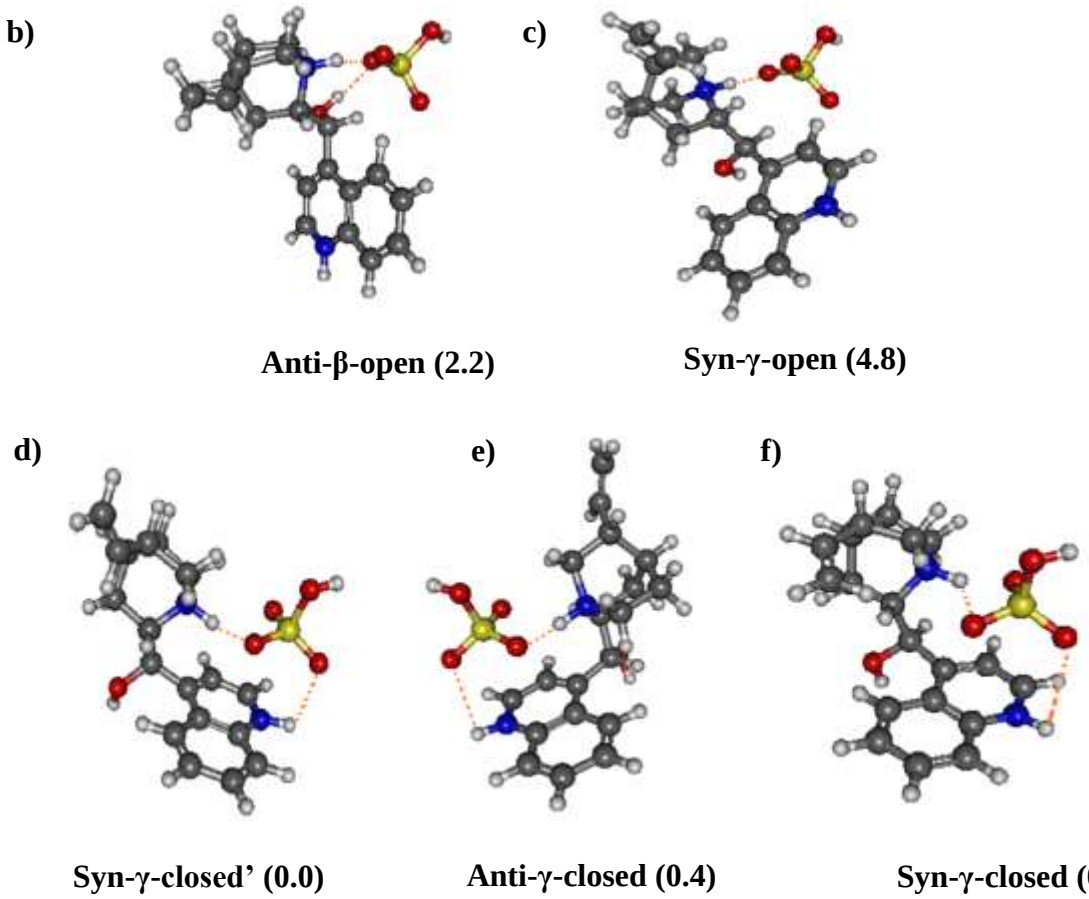

Figure 4: Structure of the five most stable conformers of the $CdH_2^{2+}HSO_4^-$ system optimized at the B3LYP-D3/6-31++G(d,p) level of theory. ***The Gibbs free energy relative to the most stable calculated complex is given in parentheses in kcal/mol***

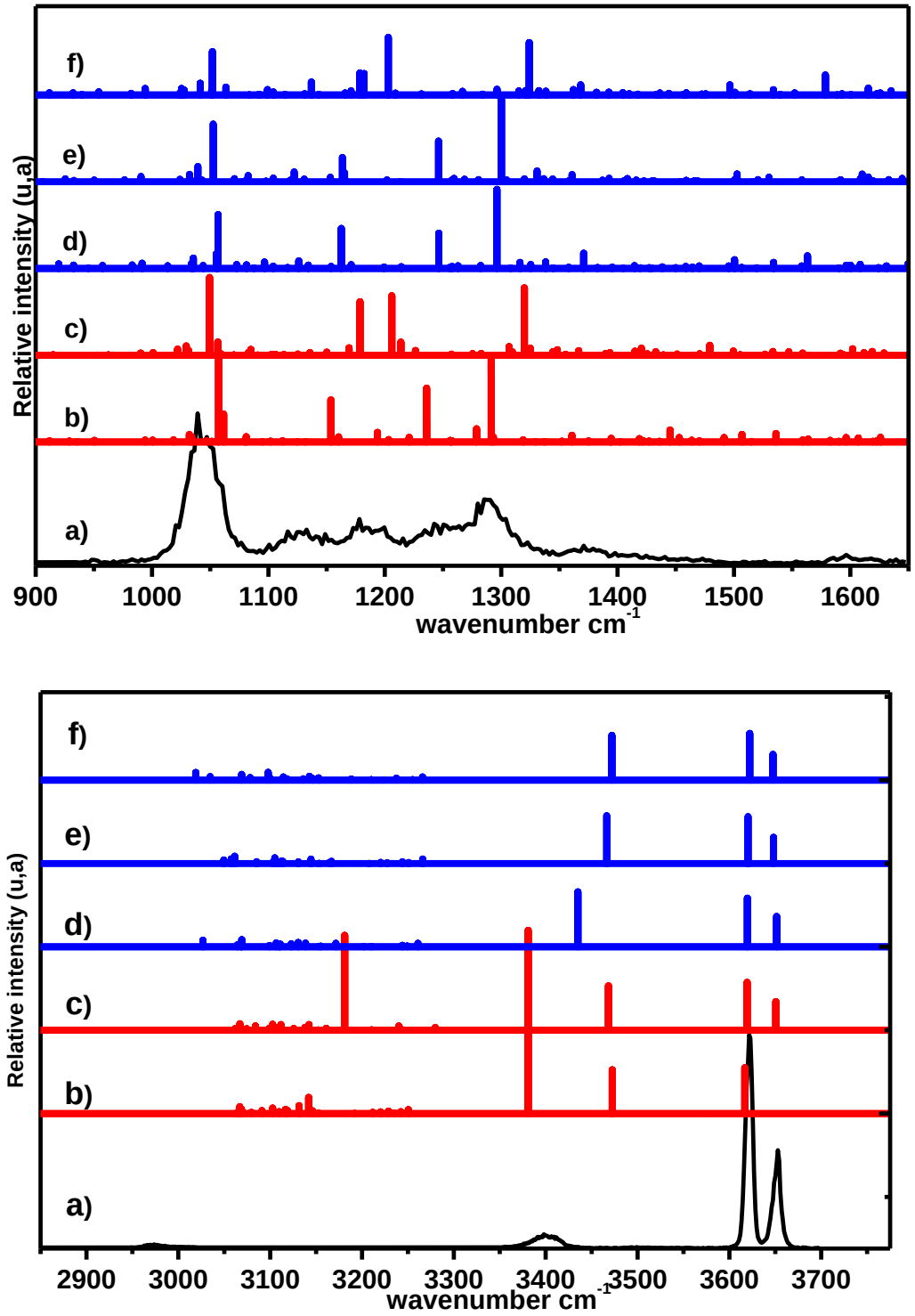

Figure 5: Comparison between the IR experimental spectrum (a) and those simulated for: b) Anti-ß-open (Figure 3b), c) Syn-γ-open (Figure 3c), d) Syn-γ-closed' (Figure 3d), e) Anti-γ-closed (Figure 3e) and f) Syn-γ-closed (Figure 3f) of the most stable conformers of $CdH_2^{2+}HSO_4^-$ system. The spectra of the open conformers are in red and those of the closed conformers in blue. Fingerprint region (Top) and high frequencies region (Bottom)

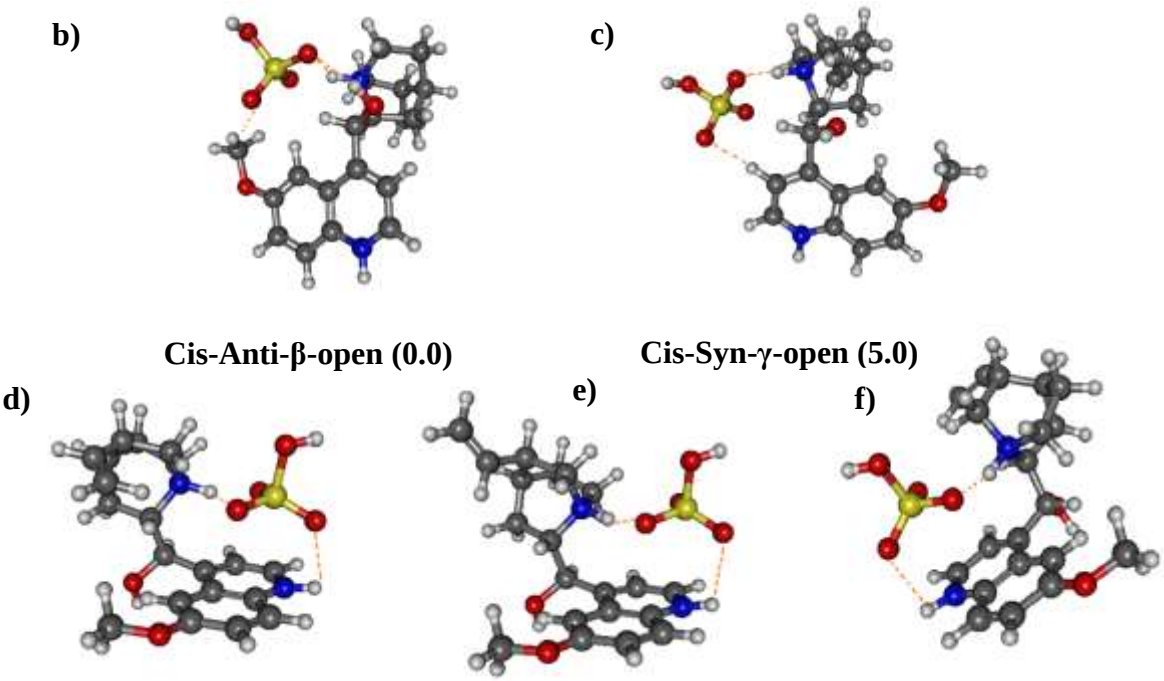

Figure 6: Structure of the five most stable conformers of the cis $QnH_2^{2+}HSO_4^-$ system optimized at the B3LYP/6-31++G(d,p) level of theory. ***The Gibbs free energy relative to the most stable calculated complex is given in parentheses in kcal/mol***

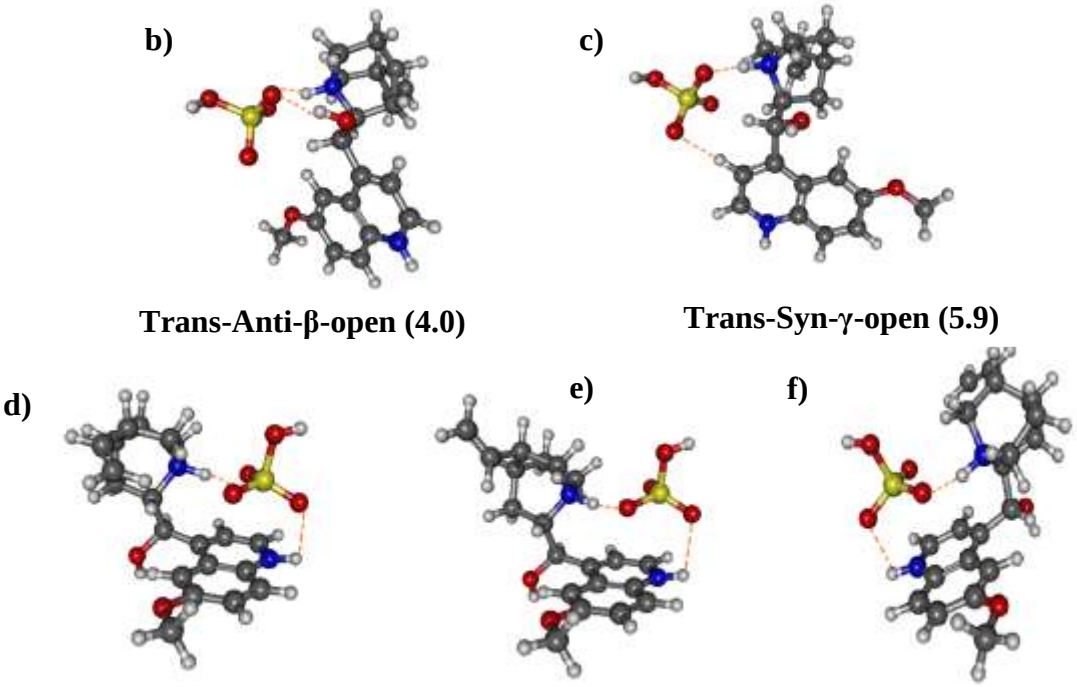

Figure 7: Structure of the five most stable conformers of the trans $QnH_2^{2+}HSO_4^-$ system optimized at the B3LYP-D3/6-31++G(d,p) level of theory. ***The Gibbs free energy relative to the most stable calculated complex is given in parentheses in kcal/mol***

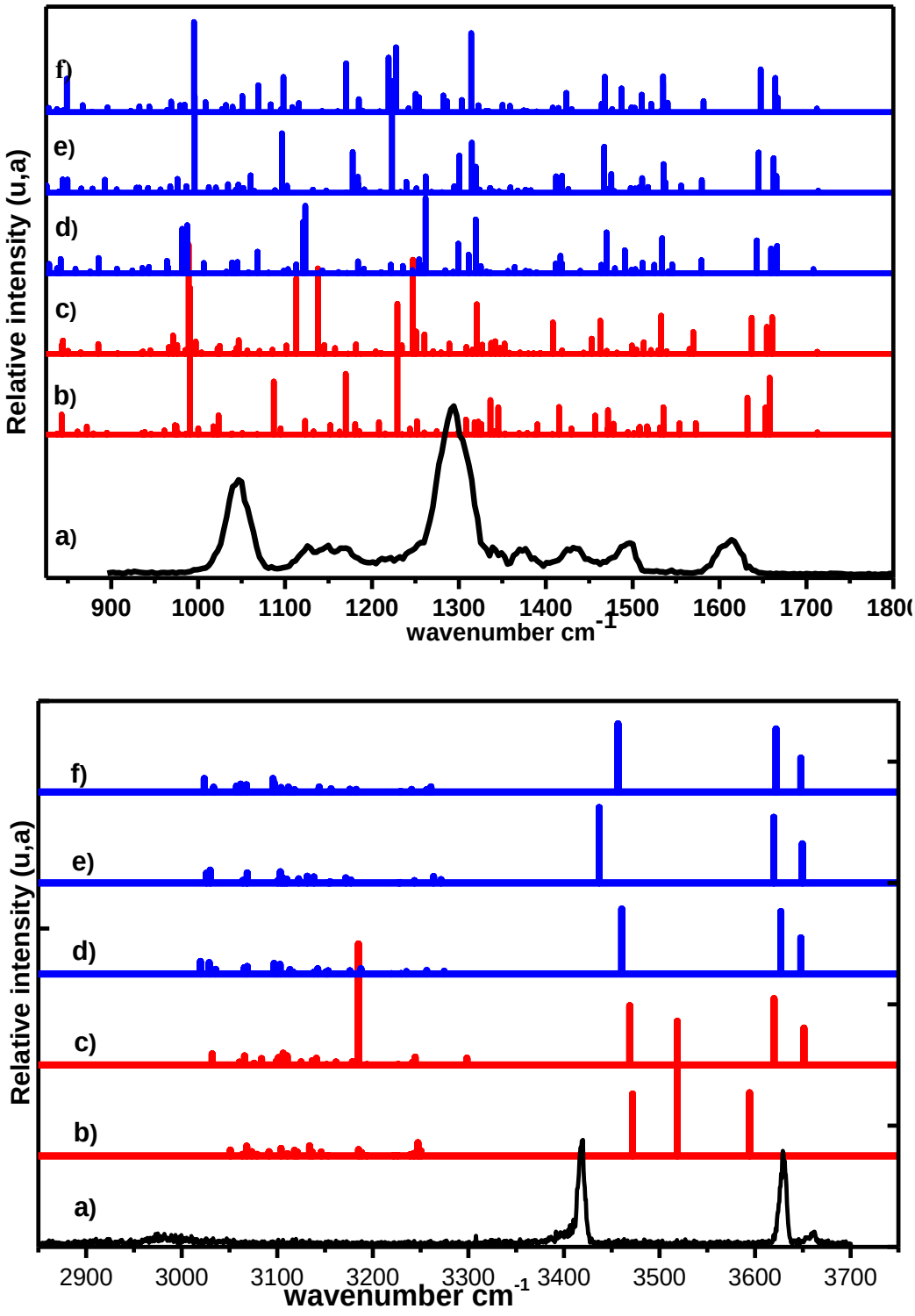

Figure 8: Comparison between the IR experimental spectrum of $QnH^{+}H_2SO_4$ (a) and the IR simulated spectra of the most stable Cis conformers: b) Cis-Anti-β-open (Figure 6b), c) Cis-Syn-γ-open (Figure 6c), d) Cis-Syn-γ-closed (Figure 6d), e) Cis-Syn-γ-closed' (Figure 6e), f) Cis-Anti-γ-closed (Figure 6f). The spectra of the open conformers are in red and those of the closed conformers in blue. Fingerprint region (Top) and high frequencies region (Bottom)

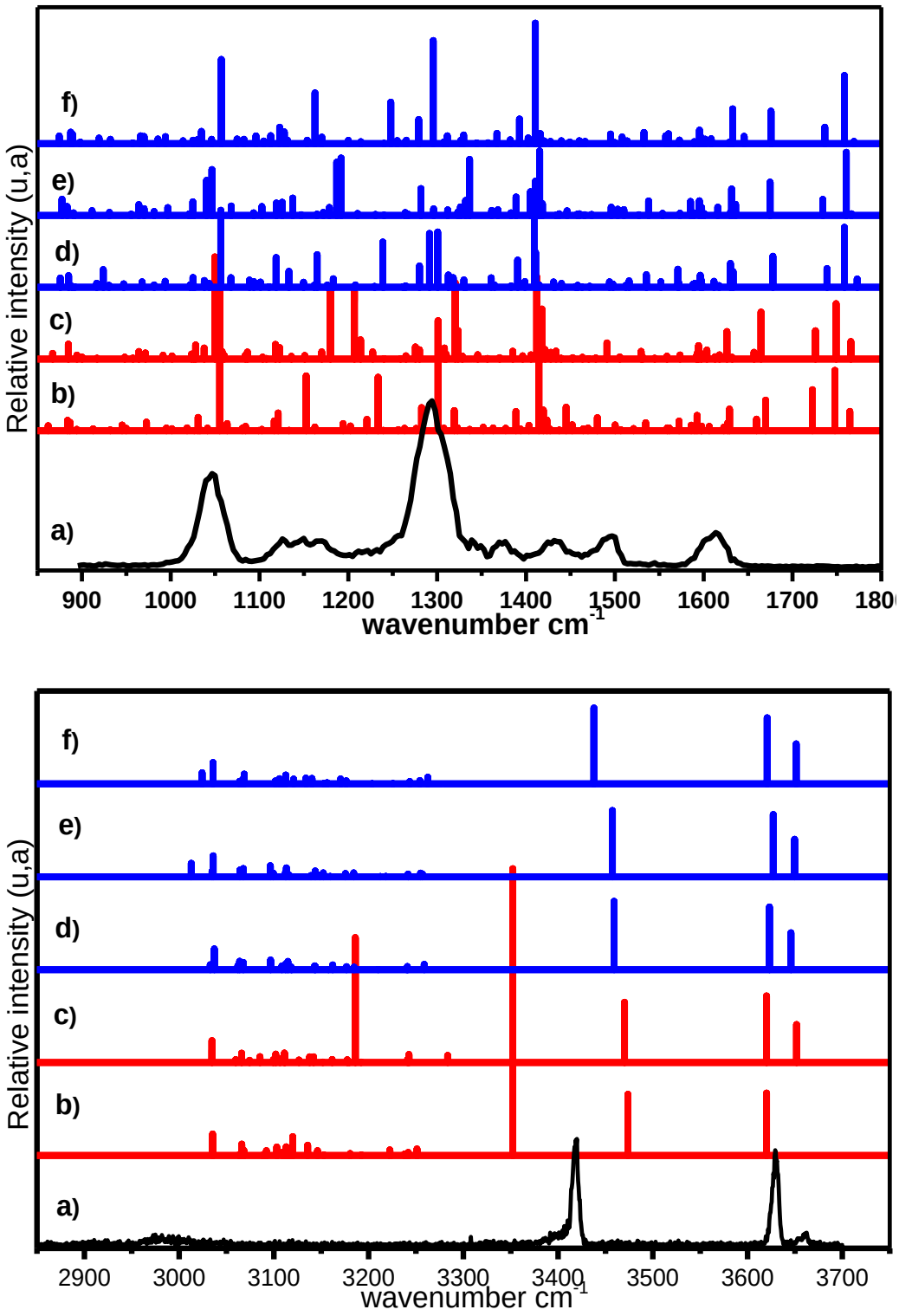

Figure 9: Comparison between the IR experimental spectrum of $QnH^+H_2SO_4$ (a) and the IR simulated spectra of the most stable Trans conformers: b) Trans-Anti-β-open (Figure 7b), c) Trans-Syn-γ-open (Figure 7c), d) Trans-Anti-γ-closed (Figure 7d), e) Trans-Syn-γ-closed (Figure 7e), f) Trans-Syn-γ-closed' (Figure 7f) The spectra of the open conformers are in red and those of the closed conformers in blue. Fingerprint region (Top) and high frequencies region (Bottom)

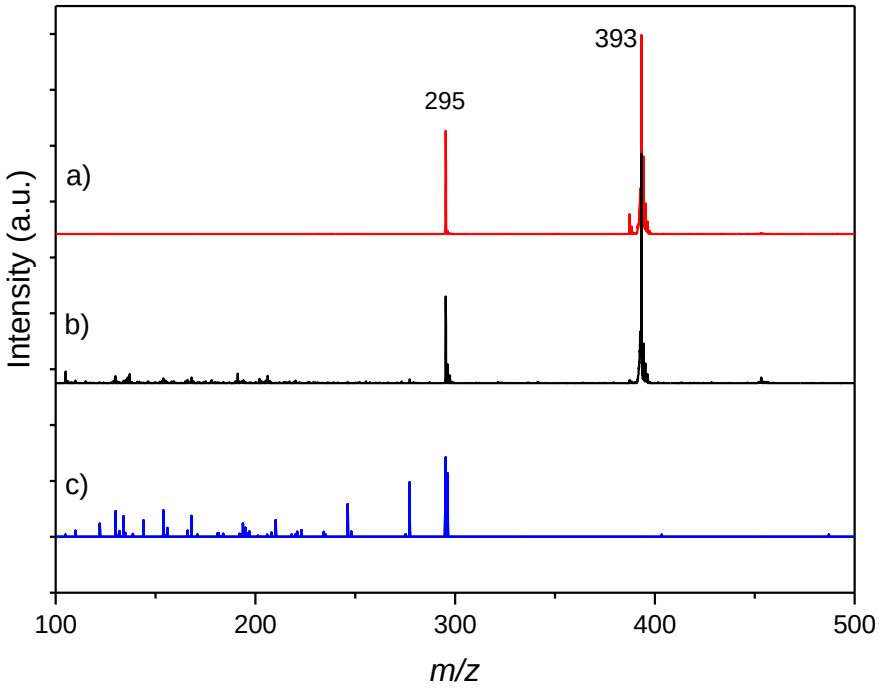

Figure 10: CID (a) and UVPD (b) mass spectra of the complex formed between protonated cinchonidine and sulfuric acid. The conditions are adjusted so that the fragmentation yield is ~0.33 in both cases. CID spectrum (c) of the m/z 295 fragment resulting from the photodissociation of m/z 393

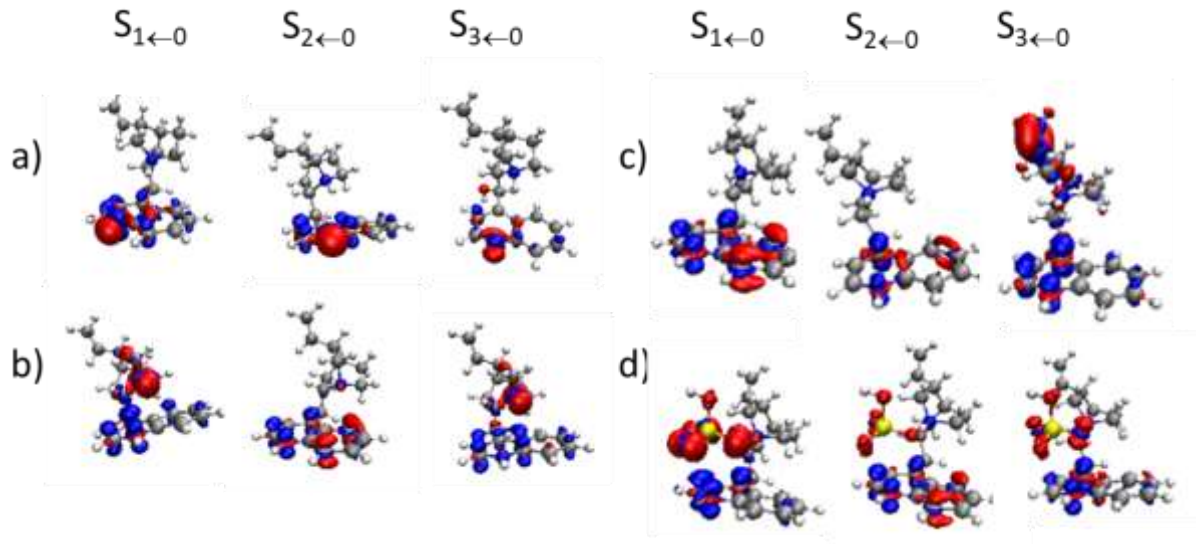

Figure 11: Difference between the electronic density of the ground state and that the first three excited states. The isolvalue is set to 0.005. The red (blue) color codes a decrease (increase) in electron density, respectively: a) CdH^+, with the proton located on N_{alk} b) $CdN_{arom}H^+$, with the proton located on N_{arom} c) CdH_2^{2+} with N_{alk} and N_{arom} protonated d) $CdH_2^{2+}HSO_4^-$ complex.

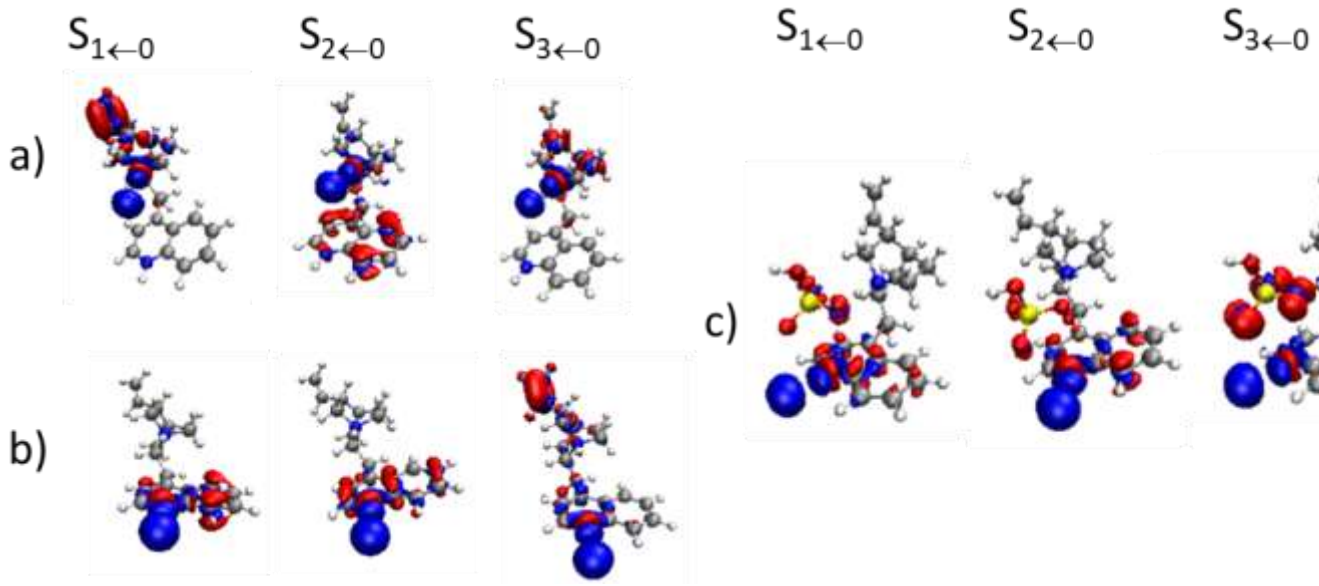

Figure 12: Difference between the electronic density of the ground state and that the first three excited states. The isolvalue is set to 0.005. The red (blue) color codes a decrease (increase) in electron density, respectively: a) CdH_2^{2+}, with $N_{alk}H$ distance of 2.0 Å b) CdH_2^{2+}, with N_{arom} H distance of 2.0 Å c) $CdH_2^{2+}HSO_4^-$ with $N_{arom}H$ distance of 2.0 Å